AEROCHEM TP-343

NASA CR-145079

ENVIRONMENTAL EFFECTS OF SPACE SHUTTLE SOLID ROCKET MOTOR EXHAUST PLUMES

By

BaoChuan Hwang and Harold S. Pergament

Prepared under Contract No. NAS1-14271

By

AeroChem Research Laboratories, Inc.

Princeton, New Jersey

for

NASA

National Aeronautics and Space Administration

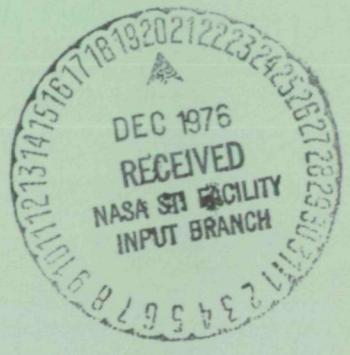

BIBLIOGRAPHIC DATA SHEET	1. Report No.	2.	3. Recipient's Accession No.
4. Title and Subtitle ENVIRONMENTAL EFFECTS OF SPACE SHUTTLE SOLID ROCKET MOTOR EXHAUST PLUMES			5. Report Date July 1976 6.
7. Author(s) BaoChuan Hwang and Harold S. Pergament			8. Performing Organization Rept. No. AeroChem TP-343
9. Performing Organization Name and Address AeroChem Research Laboratories, Inc. P.O. Box 12 Princeton, New Jersey 08540			10. Project/Task/Work Unit No. 11. Contract/Grant No. NAS1-14271
12. Sponsoring Organization Name and Address National Aeronautics and Space Administration Washington, DC 20546			13. Type of Report & Period Covered Final Report 14.
15. Supplementary Notes			

16. Abstracts The deposition of NO_x and HCl in the stratosphere from the Space Shuttle solid rocket motors (SRM) and exhaust plume is discussed. A detailed comparison between stratospheric deposition rates using the baseline SRM propellant and an 'alternate' propellant, which replaces ammonium perchlorate by ammonium nitrate, shows the total NO_x deposition rate to be approximately the same for each propellant, ranging from ≈0.018 kg/m at 15 km to ≈0.0036 kg/m at 30 km. For both propellants the ratio of the deposition rates of NO_x to total chlorine-containing species is negligibly small.

Rocket exhaust ground cloud transport processes in the troposphere are also examined. A brief critique of the NASA/MSFC Multilayer Diffusion Models (presently used for predicting pollutant deposition in the troposphere) is presented, and some detailed cloud rise calculations are compared with data for Titan III C launches. The results show that, when launch time meteorological data are used as input, the model can reasonably predict measured cloud stabilization heights.

17. Key Words and Document Analysis. 17a. Descriptors

Rocket exhaust plumes
Rocket exhaust ground clouds
Solid propellants
Computer codes
Stratosphere
Troposphere

17b. Identifiers/Open-Ended Terms

Space Shuttle
Atmospheric Interaction Plume Program
NASA/MSFC Multilayer Diffusion Model

17c. COSATI Field/Group

18. Availability Statement	19. Security Class (This Report) UNCLASSIFIED	21. No. of Pages 51
	20. Security Class (This Page UNCLASSIFIED	22. Price

Page
Intentionally
Left Blank

TABLE OF CONTENTS

LIST OF TABLES

LIST OF FIGURES

ENVIRONMENTAL EFFECTS OF SPACE SHUTTLE SOLID ROCKET MOTOR EXHAUST PLUMES

BaoChuan Hwang and Harold S. Pergament

AeroChem Research Laboratories, Inc.

I. SUMMARY

This report discusses the effects of the Space Shuttle solid rocket motor exhaust plumes on stratospheric NO_x and HCl deposition rates. The stratospheric exhaust plume predictions were made using both the AeroChem Atmospheric Interaction Plume Program (AIPP) and Low Altitude Plume Program (LAPP). The former code treats the coupled effects of nonequilibrium chemistry, gas/particle nonequilibrium and plume shocks (including the Mach disc); the latter code specifically treats the influence of nonequilibrium chemistry in the mixing/afterburning regions and is used to determine afterburning effects at the lower stratospheric altitudes. Detailed comparisons are made between stratospheric deposition rates using the baseline SRM propellant and an 'alternate' propellant which replaces ammonium perchlorate by ammonium nitrate in order to reduce the total amount of HCl in the exhaust. It was found that the total NO_x deposition rate is approximately the same for each propellant, ranging from ≈ 0.018 kg/m at 15 km to ≈ 0.0036 kg/m at 30 km. For both propellants the ratio of NO_x to total chlorine-containing species deposition rates is negligibly small, on the order of 10^{-2} for the baseline propellant and ranging from 10^{-1} to 10^{-2} for the alternate propellant. It is concluded that the alternate propellant, although it contains a large amount of ammonium nitrate, will not increase stratospheric NO_x deposition rates

The results of detailed calculations, using the AIPP code, are given for the SRM plume at 30 km altitude and demonstrate the unique capabilities of this new code.

Rocket exhaust ground cloud transport processes in the troposphere are also examined. A brief critique of the NASA/MSFC Multilayer Diffusion Models (presently used for predicting pollutant deposition in the troposphere) is presented, and some detailed cloud rise calculations are compared with data for Titan III C launches. The results show that, when launch time meteorological data are used as input, the model can reasonably predict measured cloud stabilization heights.

II. INTRODUCTION

The work reported herein is, in part, a continuation of our previous studies[1,2,3] on determining the total amount of NO_x deposited in the stratosphere by the Space Shuttle solid rocket motors (SRM). Reference 1 reported initial NO_x deposition calculations, in which the effects of (1) gas/particle nonequilibrium and nonequilibrium chemistry in the nozzle, (ii) plume shocks (including the Mach disc) and (iii) nonequilibrium chemistry in the mixing/afterburning regions and downstream of the Mach disc were taken into account. Reference 2 extended this work to study the influence (on NO_x deposition rates) of: (1) uncertainties in Al_2O_3 particle sizes, size distribution and particle/gas drag and heat transfer coefficients, (ii) intersection of the two SRM plumes and (iii) mixing (and potential combustion) of rocket exhaust products and ambient air in the shuttle base recirculation region. As a result of thse studies the total mass flow of NO_x 'leaving' the plume at 30 km altitude was determined to be 4 kg/s with a possible error factor of $\times\div$ 3. For a vehicle velocity of 1140 m/s this yields a nominal NO_x deposition rate of about 3.5×10^{-3} kg/m.

In this report we continue the above studies to determine the influence of altitude on NO_x and HCl deposition rates for both the 'baseline' and so-called 'alternate' propellants, the latter using mostly ammonium nitrate as oxidizer in place of ammonium perchlorate in order to reduce the total amount of HCl in the exhaust. Next we discuss the use of the AeroChem Atmospheric Interaction Plume Program (the AIPP code, which has been delivered to NASA/Langley) to make Space Shuttle SRM plume calculations, present detailed results for the 30 km case and show how to incorporate heterogeneous chemistry, aerosol formation and particle growth into the AIPP code. Finally, we turn our attention to an important problem involving the environmental effects of the SRM exhaust plume in the planetary boundary layer, i.e. the ground cloud generated by the SRM launch, which may result in considerable ground level pollutant deposition. A detailed examination is made of the model presently used by NASA to determine the path of the cloud and ground level pollutant (e.g., HCl) deposition rates.

The authors would like to acknowledge the assistance of Scott Wagner, Rich Gomberg, Dick Bendura, and Gerry Gregory of the NASA/Langley Atmospheric Environments Branch in explaining to us the intricacies of the Titan III ground cloud data which they obtained. In addition, Briscoe Stephens of NASA/MSFC and Arnold Goldford of Science Applications, Inc., were helpful in sending us the Univac version of the NASA/MSFC Multilayer Diffusion Model (MDM Code). Diana Buckeye of Battelle and J.R. Bjorklund of H.E. Cramer Co., explained some of the details of the code that we needed in order to convert it from Univac to operation on a CDC machine.

III. NO_x AND HCl DEPOSITION IN THE STRATOSPHERE - BASELINE AND ALTERNATE PROPELLANTS

This section discusses the influence of altitude on NO_x and HCl* deposition rates in the stratosphere for both the baseline and alternate A propellants.[4] A comparison between the propellant formulations (Table I) shows that, in the alternate propellant, ammonium nitrate has replaced most of the ammonium perchlorate which should result in substantially decreased HCl concentrations at the nozzle exit plane. Interestingly enough, although we might expect that the large amount of ammonium nitrate might result in significantly larger amounts of NO_x produced in the chamber, equilibrium calculations (Table II) show that this is not the case. In fact, the NO mole fraction is observed to be about a factor of 50 less than that for the baseline propellant, primarily because of the substantially decreased chamber temperature. However, the question arises of whether, because of the ammonium nitrate in the propellant,† equilibrium values of NO_x will in fact be achieved in the chamber. (It is well known[5,6] that in laboratory flames and furnaces, above-equilibrium levels of NO_x are reached.) This question is addressed below.

A. Combustion Chamber Analysis of NO_x Concentrations

The model used for these calculations assumed that all exhaust products, except the nitrogen-containing species, reached their equilibrium levels at the computed adiabatic flame temperature. For conservatism, we assumed that 25% of the N in the propellant was initially converted to NO‡ (note that at equilibrium only 0.1% of the N in the propellant is converted to NO), the remaining N going to N_2. A constant pressure, constant temperature, nonequilibrium chemistry calculation was then made in which the nitrogen-containing species concentrations were determined by solving the species conservation equations using the initial conditions given in Table III and the reaction mechanism in Table IV. Figure 1 shows the computed NO mole fraction (X_{NO}) as a function of time (labeled FIRST ASSUMPTION). It is seen that X_{NO} approaches its equilibrium value in about 5 ms. In order to determine whether equilibrium will be achieved in the chamber the above reaction time must be compared with a characteristic flow time. For an average gas velocity in the chamber of 91.5 m/s§ the time to traverse

---

* Almost all the chlorine in the exhaust plume is tied up as HCl, although a small percentage appears as Cl and Cl_2. When the term HCl is used in the text it refers to the total chlorine-containing species.

† Of equal importance is that the atomic mass fraction of N in the alternate propellant is about a factor of 2 larger than the corresponding value for the standard propellant.

‡ Because of this assumption some O had to be removed from the remaining O-containing species. This was accomplished by arbitrarily reducing the mole fraction of H_2O by an appropriate amount.

§ This was computed from the SRM mass flow, the density of the combustion products and the approximate cross sectional area of the chamber.

the approximately 61 m length of the chamber is about 700 ms. Therefore we expect that NO_x equilibrium will be achieved under these conditions. In order to get an approximate upper limit to X_{NO} in the chamber the rate coefficients were arbitrarily decreased to their estimated lower bounds (as noted in Table IV). These results, labeled in figure 1 as, MOST CONSERVATIVE, show that within about 20 ms (1.8 m) equilibrium is reached in the chamber.

In order to determine the reasonableness of the assumptions used in this model, two additional calculations were made in which the temperature was arbitrarily reduced to 2000 K and 1500 K. These results, also shown in figure 1, indicate that at temperatures typical of laboratory flames and furnaces, NO is computed to freeze at above equilibrium values, in accord with what is known about these lower temperature systems.[5,6] These results demonstrate that NO reaches equilibrium primarily because of the high rocket chamber temperature, and we conclude that the computed equilibrium chamber value of X_{NO} for the alternate propellant is a reasonable starting point for the subsequent nozzle and exhaust plume calculations.

B. Influence of Altitude on NO_x Deposition Rates

A calculation procedure similar to that described in reference 1 to determine the NO_x deposition rate at 30 km was used to determine the corresponding value at 15 km. Qualitatively, the principal differences in the overall plume structure at these two altitudes are (i) at the lower altitude the effects of afterburning are more severe and (ii) the plume is less underexpanded at 15 km, changing the shock locations, the size of the Mach disc and therefore the mass flow of exhaust gases passing through the Mach disc.

As discussed in reference 1 the amount of NO_x 'leaving' the plume can be greater than that leaving the nozzle (the so-called plume enhancement) due to both afterburning and shocks. The total NO_x deposition rate can be related to the mass flow of NO_x leaving the nozzle by defining an overall plume enhancement factor (OPEF),

$$OPEF = \frac{(\dot{m}_{NO_x})_T}{(\dot{m}_{NO_x})_{ex}} \tag{1}$$

where $\dot{m}_{NO_x}$ is the mass flow of NO_x, subscript T signifies the total amount leaving the plume and subscript ex signifies the amount leaving the nozzle. For the purpose of determining the influence of altitude on NO_x deposition it is reasonable to assume that the NO_x produced by shocks and afterburning are independent quantities and can be separately calculated. Then the predicted NO_x deposition rate obtained by adding the NO_x produced by shocks and afterburning individually will give a conservative upper bound to the real NO_x deposition. Defining total mass flow of NO_x separately for shocks and afterburning gives,

$$(\dot{m}_{NO_x})_{T,SH} = (\dot{m}_{NO_x})_{ex} + (\dot{m}_{NO_x})_{SH} \tag{2a}$$

$$(\dot{m}_{NO_x})_{T,SH} = (\dot{m}_{NO_x})_{ex} + (\dot{m}_{NO_x})_{AFT} \tag{2b}$$

Then, defining individual OPEF's for afterburning and shocks gives

$$(OPEF)_{SH} = \frac{(\dot{m}_{NO_x})_{T,SH}}{(\dot{m}_{NO_x})_{ex}} \tag{3}$$

$$(OPEF)_{AFT} = \frac{(\dot{m}_{NO_x})_{T,AFT}}{(\dot{m}_{NO_x})_{ex}} \tag{4}$$

From the above definitions it is evident that,

$$OPEF \leq (OPEF)_{SH} + (OPEF)_{AFT} + 1 \tag{5}$$

Equation (3) can be rewritten as

$$(OPEF)_{SH} = 1 + \frac{(Y_{NO_x})_{MD}}{(Y_{NO_x})_{ex}} \left(\frac{\dot{m}_{MD}}{\dot{m}_{ex}} \right) \tag{6}$$

where $(Y_{NO_x})_{MD}$ and $(Y_{NO_x})_{ex}$ are the mass fractions of NO_x downstream of the Mach disc and at the exit plane respectively and $\dot{m}_{MD}$ and $\dot{m}_{ex}$ are the mass flows passing through the Mach disc and leaving the nozzle, respectively. The use of equation 6 alone to establish the enhancement of NO_x due to shocks implies that the major increase is due to the first Mach disc. The other shocks (exhaust gas and air shocks and subsequent Mach discs) are assumed to contribute a negligible amount to the total plume NO_x enhancement. This assumption is quite adequate for the plumes of interest (see, e.g. ref. 2).

An examination of equation 6 clearly shows that $(OPEF)_{SH}$ depends on two factors; (1) the increase in NO_x mass fraction due to the high post-shock temperature (approximately equal to the combustion chamber temperature) and (2) the amount of propellant exhaust product mass flow passing through the Mach disc. The first factor is primarily controlled by thermodynamics, since we have already shown[1] that the NO_x mass fraction rapidly achieves a state of near local thermochemical equilibrium at the pressure and temperature downstream of the Mach disc. The second factor is controlled by the gas dynamic plume structure, and is a function primarily of the nozzle exit to ambient pressure ratio and the nozzle exit Mach number. To get a feeling for numbers, if there was an order of magnitude increase in Y_{NO_x} through the Mach disc and 10% of the total mass flow passed through the Mach disc, $(OPEF)_{SH} = 2$.

The OPEF for afterburning can be written as,

$$(OPEF)_{AFT} = 1 + \frac{(\dot{m}_{NO_x})_{AFT}}{(\dot{m}_{NO_x})} \tag{7}$$

or

$$(OPEF)_{AFT} = 1 + \frac{4\pi \int_0^{\infty} \rho u \, Y_{max} \, r dr}{(Y_{NO_x})_{ex} \, \dot{m}_{ex}} \qquad (8)$$

where ρ and u are the gas density and velocity respectively and r is the radial distance from the axis. From equation 8 it is observed that the influence of afterburning on plume NO_x enhancement must be determined via a radial integration of NO_x profiles through the plume.

Initial conditions for afterburning calculations at 15 km made using the AeroChem LAPP code[7] are given in Table V. The radius of 8.23 m is an 'expanded' radius for an equivalent single nozzle plume--expanded from the actual exit condition, $p \approx 10^5$ Pa, $R_{ex} = 1.83$ m to the ambient pressure of 1.21×10^4 Pa. Figure 2 shows the large temperature increase due to afterburning at this altitude for both the baseline and alternate propellants (compare these results with figure 11 of reference 1 which shows no temperature increase at 30 km for the baseline propellant). The local plume enhancement factor due to afterburning (which is simply equation 8 evaluated as a function of downstream distance) is shown to be considerably larger for the alternate propellant than for the baseline propellant. This is primarily because $(Y_{NO_x})_{ex,ALT}$ is about a factor of 50 less than $(Y_{NO_x})_{ex,BASE}$. The actual NO_x mass fractions produced in the afterburning plumes of both propellants are about the same.

Table VI gives the results of the OPEF calculations showing the relative effects of shocks and afterburning for both the baseline and alternate propellants. As expected, because of increased reaction rates resulting in greater heat release in the plume, the effects of afterburning are greater at 15 km than at 30 km. The enhancement for the alternate propellant is greater than that for the baseline primarily because the mass flow of NO_x leaving the nozzle is very much less than that of the baseline propellant (see exit plane composition in Table V).

The absolute amounts of NO_x deposited in the stratosphere are shown in Table VII. It is observed that these are about the same for each propellant, the values being about a factor of from 3 to 5 higher at 15 km than at 30 km.

C. Comparison between NO_x and HCl Deposition Rates

Since both NO_x and HCl participate in the ozone destruction cycle (NO_x less efficiently than HCl), of primary interest is the ratio of NO_x to HCl deposition rates in the stratosphere. Since there are no major sources or sinks for the total amount of chlorine contained in the exhaust products, the mass flow of HCl leaving the plume is approximately equal to that leaving the nozzle. Table VIII gives both the total NO_x deposition rate (in kg/m for use in statospheric diffusion models which use pollutant deposition as a source term) and the ratio of NO_x to HCl deposition. These results show that the amount of NO_x deposited in the stratosphere is negligibly small compared to the HCl deposited,* the NO_x/HCl ratio ranging from values on the order of 10^{-1} to the order of 10^{-3}.

---

* Note that this is the case even using the upper bound calculation described above.

IV. COMPUTATION OF EXHAUST PLUME PROPERTIES

This section discusses the use of and results from a new computational tool developed by AeroChem to compute rocket exhaust plume properties, taking into account the coupled effects of nonequilibrium chemistry, turbulent mixing, gas/particle dynamic and thermal nonequilibrium and plume shocks. This code, the Atmospheric Interaction Plume Program (AIPP)[8,9] was written with support from the Air Force Rocket Propulsion Laboratory and has been applied here to the determination of stratospheric SRM plume properties.

A. Delivery and Use of the AIPP Code

The AIPP code was delivered to the NASA/Langley Research Center and demonstrated to operate on the CDC 6600 computer facility. Complete documentation of the code (both user oriented and program oriented) is given in AeroChem TP-302a and TP-328, which have been updated and submitted as the Computer Programming Documentation, together with a source language deck of the code and test case input and output.

Use of the code requires that detailed nozzle exit plane gas and particle properties be specified as initial conditions together with the vehicle flight velocity and altitude, a suitable chemical reaction mechanism and rate coefficients. The proper nozzle exit plane conditions can be obtained via the AeroChem fully-coupled nozzle code (FULLNOZ)[10] which outputs exit plane gas and particle properties in a form directly usable as input to the AIPP code.

B. Calculations Using the AIPP Code

The AIPP code has been used to calculate complete SRM exhaust plume properties at 30 km for a flight Mach number of 3.8. Calculations were made for an equivalent single nozzle (with a mass flow equal to the total mass flow of the two SRM's). Distributions of gas and particle properties at the nozzle exit plane (computed via FULLNOZ) are given in figures 3 to 5. The rather large decrease in gas temperature toward the nozzle lip occurs at the limiting particle streamline (i.e. there are no particles at radii greater than the radius at which the limiting particle streamline occurs). Table IX gives the chemical reaction mechanism and rate coefficients used for the plume calculations. The shock structure in the plume is given in figure 7, together with the computed mixing/afterburning region and the dividing streamline (DSL) in the subsonic/supersonic (SS) region which separates the exhaust gas passing through the Mach disc from the exhaust gas which has passed through both the exhaust gas shock and reflected shock. The DSL in the SS region is seen to resemble a convergent nozzle until the point where the initially subsonic flow turns supersonic. Figures 7 and 8 give the centerline distributions of temperature, Mach number, pressure and NO_x mole fraction. As expected, the pressure drops well below the ambient pressure just upstream of the Mach disc and then increases to about a factor of 2 greater than ambient after passing through the normal shock. The subsequent pressure distribution is observed to rapidly approach the ambient level.*

---

* In reference 9 it is pointed out that the AIPP code does not handle multiple normal shocks downstream of the Mach disc.

The temperature immediately downstream of the Mach disc increases to approximately the combustion chamber value and then, because the flow is far out of nonequilibrium, rapidly dissociates with a large temperature decrease. The centerline mole fraction of NO_x (fig. 8) increases to a peak value that, because of the rapid dissociation, is less than the equilibrium value at the post-shock pressure and temperature.

The radial plots of X_{NO_x} (fig. 9) are indicative of the total NO_x mass flow, i.e., $\dot{m}_{NO_x} \propto \int_0^\infty \rho u \, X_{NO_x} \, r dr$, at any axial location. This mass flow is then divided by the exit plane NO_x mass flow to get the Local Plume Enhancement Factor (LPEF). Finally, the asymptotic value of the LPEF is the OPEF, which gives the total NO_x deposition rate. A comparison between the OPEF computed via the AIPP code and that computed from the 'equivalent AIPP' calculations of reference 1 shows that the results are similar.

C. Heterogeneous Chemistry, Aerosol Formation, Particle Growth and Coagulation

1. Heterogeneous Chemistry

In this work we have concentrated on developing a formal technique for incorporating heterogeneous chemistry within the AIPP code, particularly radical recombination reactions taking place on the surface of Al_2O_3 particles. These reactions, by increasing the rate of recombination of e.g., H, OH, Cl, could reduce these species concentrations to a level low enough to 'suppress' afterburning.

Our heterogeneous chemistry model is a phenomenological one which relates the recombination rate at the particle surface to the arrival rate of molecules and the surface sticking probability. Thus we define a 'heterogeneous rate coefficient' for the following general type of one-way reaction

$$R_1 + R_2 + S \rightarrow P + S$$

where R_1 and R_2 are radicals, P is the recombination product and S represents the particle surface. The rate equation then becomes,

$$\frac{d[R_1]}{dt} = \frac{d[R_2]}{dt} = -k_{HET}[R_1][R_2][S] \tag{9}$$

where $[R_1]$ and $[R_2]$ are the number densities of R_1 and R_2 respectively and [S] is the particle number density. If we assume that the particle diameters are small compared to the gas mean free path, then the arrival rate of molecules at the surface is simply the random flux of molecules across a surface, determined from kinetic theory. Using this assumption, the rate equation becomes,

$$\frac{d[R_1]}{dt} = \frac{d[R_2]}{dt} = -\pi \, r_{p_i}^2 \left(\frac{8kT}{\pi \, m_{R_1}}\right)^{1/2} \left(\frac{8kT}{\pi \, m_{R_2}}\right)^{1/2} [R_1][R_2][S_i] \tag{10}$$

where r_{p_i} is the radius of the ith particle group, m_{R_1} is the mass of R_1, k is the Boltzmann constant and T is gas temperature.

Utilizing equations 9 and 10 and defining a sticking probability, η_S, to account for the fact that not all molecules will stick to the particle surface gives the following expression for k_{HET},

$$k_{HET} = \pi r_{p_i}^2 \eta_S \left(\frac{8kT}{\pi m_{R_1}}\right)^{1/2} \left(\frac{8kT}{\pi m_{R_2}}\right)^{1/2} \tag{11}$$

In a practical sense, all radicals in the flow can recombine at particle surfaces and a heterogeneous reaction mechanism (Table X) must be added to the gas phase reactions given in Table IX.

The formal method of incorporating a heterogeneous reaction scheme into AIPP is given below:

1. A subroutine must be added to the code[9] (to be called from CHEM) to evaluate the heterogeneous rate coefficient, k_{HET}, for each reaction and each particle group. This routine must take input data on η_S for each reaction, as well as particle number densities and species concentrations (which are available in COMMON).

2. The reactions are input as one-way, two-body reactions of type 9 (see ref. 9) since [S] and k_{HET} will be lumped together as one term which will multiply the particle concentrations.

A similar procedure has been used by AeroChem[11] to analyze ion/electron recombination on liquid droplets with application to the injection of water and electrophilic liquids into re-entry plasma sheaths to alleviate communications blackout.

2. Aerosol Formation, Particle Growth and Coagulation

In addition to the influence of solid particles in enhancing radical recombination, they can also act as nucleation sites for the condensable species in the exhausts. Condensation can also, of course, be initiated via homogeneous nucleation in the plume, i.e., the kinetic formation of 'critical size' nuclei. However, considering the large particle number densities and ion densities (which can also induce nucleation), it is likely that heterogeneous nucleation will prevail. Heterogeneous nucleation rates can be calculated in a manner similar to that described in Section IV.C.1 above, assuming that each collision at a particle surface results in the condensible species being assimilated into the particle, i.e., the sticking probability is unity. The rate of disappearance of the gas phase can then be written as,

$$\frac{d[c]}{dt} = - \pi r_p^2 \left(\frac{8kT}{m_L}\right)^{1/2} \tag{12}$$

where m_L is the mass of the condensable species.

a. Particle Growth - When the condensate particles are small, e.g., formed by heterogeneous nucleation via ions, the condensation rate and therefore the rate of particle growth is controlled via chemical kinetic processes. When the particles are sufficiently large that the Knudson number (ratio of mean free path to particle diameter) in the flow falls below unity, the particle growth (condensation) process is controlled by diffusion of the condensing species through the boundary layer surrounding the droplet. Basically, the problem

reduces to one of determining the rate of heat transfer from and mass transfer to a spherical droplet within a surrounding gas stream--exactly the opposite of the 'evaporating' droplet problem.

A chemical kinetic approach to the growth phenomena was suggested by Jensen[12] who studied the growth of carbon particles, formed by homogeneous nucleation, in a liquid rocket motor containing the monopropellant, isopropryl nitrate. Jensen suggested several possible 'growth' species, defined as "molecules which are assimilated into a particle, physically or chemically, upon collision of the molecule with the particle surface." In formulating a 'rate coefficient' to calculate the total rate of depletion of the growth species it was assumed that each collision of a growth species at a particle surface results in assimilation of the growth species into the particle (similar to the assumption leading to equation 12).

The problem of calculating particle growth when the particles are large enough to have a significant boundary layer and their growth is controlled by diffusion of the condensing gas species is one of extreme mathematical difficulty which has not been solved 'exactly' except for either very small or large Reynolds numbers. There have been, however, some successful approximations (see, e.g. ref. 13). The, more or less, classical approach is to relate a set of dimensionless parameters containing the heat and mass transfer rates to the flow properties. These parameters are Reynolds number (Re), Nusselt number (Nu), Sherwood number (Sh), Prandtl number (Pr), and Schmidt number (Sc), defined as:

$$Re = \frac{\rho_e u_e d}{\mu} \tag{13}$$

$$Nu = \frac{q_o d}{A(T_o - T_e)k} = \frac{hd}{k} \tag{14}$$

$$Sh = \frac{\dot{m} d}{A(C_e - C_o)D} \tag{15}$$

$$Pr = \frac{\mu c_p}{k} \tag{16}$$

$$Sc = \frac{\mu}{\rho D} \tag{17}$$

The following nomenclature is used in the above equations:

d is particle diameter, μ is gas viscosity, q_o is heat transfer to the particle surface, k is gas thermal conductivity, T is gas temperature, h is the standard heat transfer coefficient, $\dot{m}$ is the mass transfer rate, D is the diffusion coefficient, C is species concentration, c_p is specific heat and subscripts 'e' and 'o' refer to the edge of the boundary layer and the particle surface, respectively.

From similarity it can be shown that,

$$Nu = f_1(Re, Pr) \tag{18}$$

$$Sh = f_2(Re, Sc) \tag{19}$$

Employing the above formulation reduces the basic problem of determining the deposition of a condensing vapor on a particle to that of determining the functions f_1 and f_2. Considerable theoretical and experimental work has been done on this fundamental problem covering a wide range of Reynolds numbers (see, e.g. ref. 14). For $10^2 < Re < 10^5$, a laminar boundary probably exists over the front face of a spherical particle; the flow behind the particle is the 'usual' type of wake flow. At higher Re, transition to turbulent flow will occur (the precise value depending in part on the 'freestream' turbulence level). A reasonable semi-empirical expression for the condensation rate can be obtained from[13]

$$Sh = 2(1 + \beta\ Re^{1/2}\ Sc^{1/3}) \tag{20}$$

which is analogous to the familiar heat transfer expression

$$Nu = 2(1 + \beta\ Re^{1/2}\ Pr^{1/3}) \tag{21}$$

where β has been empirically determined to be about 0.3.

The implementation of expressions for the Sherwood number (similar to equation 20) to calculate the actual growth of droplets within a solid propellant exhaust plume is relatively straightforward within the framework of a computer model using a finite difference formulation of the governing equations (e.g., the AeroChem AIPP code[9]). Combining equations 15 and 17 gives, for a spherical particle,

$$\dot{m} = 2\pi d(C_e - C_o)D[1 + \beta\ Re^{1/2}\ Sc^{1/3}] \tag{22}$$

Although the particle diameter is increasing with time the quasi-steady approximation, which assumes the time-dependent rate of change of surface area, $\partial A/\partial t$, is much smaller than that computed from the condensation rate $\dot{m}$, may safely be employed. Using the local flow conditions and initial droplet diameter, d_i, a new droplet diameter d_f at the end of a given integration step, Δt, can be computed from

$$\frac{\pi}{6}\left[d_f^3 - d_i^3\right]\rho_p = \dot{m}\Delta t \tag{23}$$

where ρ_p is the particle density. In this step by step manner the increase of droplet diameter can be determined throughout the plume. In the AIPP code[9] this analysis should be added to subroutine PART.

b. Particle Coagulation - It is expected that condensate particles will coalesce or stick together if they come in contact. This coagulation process is well known and it can be shown[15] that the rate at which particles disappear by coagulation can be expressed by,

$$\frac{dn}{dt} = -Kn^2 \tag{24}$$

where n is the number of particles per cm^3. The classic approach to determining the kinetics of coagulation is the theory of Smoluchowski[16] who proposed that particles collide due to Brownian motion and that the particles stick to each other in a certain fraction of those collisions. For all particles of the same size the Smoluchowski expression reduces to

$$K = \frac{2}{3}\frac{R\,T\,s}{\mu\,N} \tag{25}$$

where R is the universal gas constant, N is Avogadro's number and s is the ratio of the sphere of influence to the radius of the particle (which, if greater than unity, assumes that particles will coagulate even before touching). A routine to determine the coagulation of particles can readily be added to subroutine PART in the AIPP code.[9]

V. SRM GROUND CLOUD RISE AND ATMOSPHERIC DIFFUSION MODELS

This section reports on the initial results of a long term study to determine the accuracy of existing models to predict both the path of the SRM ground cloud and the deposition of pollutants along the path. The study is aimed at assessing the environmental impact of Space Shuttle operations with respect to the influence on the troposphere and on ground level pollutant concentrations (particularly HCl and particulates) in the vicinity of the Kennedy Space Center. The need to understand and predict these environmental effects led to the development of the NASA/MSFC Multilayer Diffusion Model (MDM). This model is described in great detail in reference 17 and some calculated results of ground cloud rise, cloud path and HCl downwind deposition for some Titan III launches have been reported in e.g. reference 18. However, the assumptions incorporated into the MDM (reviewed in Section V.A below), led to concern that there might be wide error bands on the predicted results. Since it is anticipated that the MDM is to be used during the Shuttle launch countdown in order to determine whether a potential launch hazard exists, it is necessary to minimize these error bands. Thus, our work is directed toward the determination of (1) those meteorological conditions for which the MDM is likely to give results that either underpredict the actual hazard or are too conservative and (2) a method by which the present model can be modified to give more realistic predictions of the ground cloud path and pollutant deposition rates.

Our overall approach toward accomplishing the above goals is to first, make a detailed, critical analysis of the MDM code in order to understand its strengths and weaknesses and its explicit and implicit assumptions; second, to compare calculated results from the MDM code with more exact 'numerical' models (e.g. the Lawrence Livermore ADPIC code[19]) and the available data (e.g. ref. 20) on Titan III launches* under a wide variety of meteorological conditions and third, as a result of the above steps determine the magnitude of

---

* Titan III is used for the environmental effects study because it uses the same propellant as the SRM and is about 1/2 the thrust. The interpretation of these data is therefore very significant with regard to the SRM ground cloud study.

the errors in predicting the concentration and dosage fields (for different weather conditions) resulting from transport of the Shuttle ground cloud exhaust products as they move downwind in the earth's surface mixing layer. In this section it is assumed that the reader has a general familiarity with both rocket exhaust ground cloud dispersion problems and with the MDM code. Additional information on these topics can be found in references 21 and 22.

The work reported below is the first part of the overall program to validate the MDM code in the manner described above; it will be continued over the next year under Contract NAS1-14504.

A. NASA/MSFC Multilayer Diffusion Model (MDM)

The basic code includes two programs which describe two different physical processes; the first describes the buoyant force dominated cloud rise while the second describes the diffusion processes controlled by atmospheric turbulence.

1. Cloud Rise

The hot exhaust products formed during rocket launches rise due to buoyancy. The exhaust cloud of pollutants mixes with ambient air because of the velocity shear between the cloud gases and the air. This entrainment of cool air has a critical effect on cloud rise since it reduces the buoyant force. In stable and neutral atmospheres, the cloud will rise to a stabilization height where it is in thermal equilibrium with the ambient environment, following which atmospheric turbulence will dominate the subsequent transport process, i.e., further motions of the cloud will be controlled by both the wind velocity and turbulent diffusion.

The NASA/MSFC models for predicting cloud rise are based on the work of Briggs[23,24] who developed formulae for stack plumes. The NASA/MSFC MDM incorporates two types of cloud rise models: (1) instantaneous cloud rise models which assume spherical entrainment (designed to apply to normal launches of solid-fueled rocket vehicles, e.g., Space Shuttle, Titan III, Minutemen II, etc.) and (2) continuous cloud rise models which assume cylindrical entrainment (used for the cloud rise from vehicles with liquid-fueled first stages). For a vehicle using both liquid and solid fuel engines, e.g., the Delta-Thor, the authors of the code[17] recommend an average of the rise predicted using the instantaneous and continuous cloud rise models.

Since the net effect on buoyant cloud rise of atmospheric entrainment due to turbulence is not well known and the large velocity fluctuations due to convective eddies in unstable air cause severe measurement problems, no adequate formula for predicting cloud rise in unstable conditions presently exists. Thus, the cloud rise program utilizes the same formula for both unstable and neutral atmospheres.

Derivations of all models in the NASA/MSFC cloud rise program can be found in the report by Dumbauld et al.[22] The original Briggs model is based on (1) the conservation equations for buoyancy and momentum, (2) the assumption

that the plume grows linearly* (the entrainment assumption), (3) the equivalency between the mean horizontal speed of the plume in the bent over stage and the ambient wind speed, and (4) a constant stability parameter S. The entrainment constant for the linear growth of the radius of the rising cloud is still a controversial number.[25] The value of 0.64 used in the NASA/MSFC models is based on a best fit for a bulk of empirical measurements on stack plumes. Certainly, a check of this value against the rocket exhaust cloud is needed since the entrainment constant may not be the same for rising plumes which have been generated by different means.[26]

In addition to incorporating the Briggs model for the path of the mass center of the rising cloud, the NASA/MSFC cloud rise models also provide calculations of the dimensions and spatial positions of the ground cloud at stabilization and the distribution of exhaust products which are required input in the NASA/MSFC diffusion models. At present only the input information from MDM models 3 and 4 (see Section V.A.2 below) are given in the cloud rise models. It is assumed that the pollutant concentration distribution of the stabilized cloud is Gaussian. The center of the Gaussian distribution is at the cloud stabilization height, calculated using Briggs' formula. Assuming that the pollutant concentration at a distance of one radius, r, from the cloud stabilization height, Z_m, is 10% of the concentration at Z_m, the standard deviation of the Gaussian distribution can be given as r/2.15. From the entrainment assumption in Briggs' formula $r = \gamma \cdot Z = 0.64Z$, where γ is the entrainment constant defined above. Since the portion of the cloud above the mixing layer height (also referred to as the inversion height) is dominated by a convective mechanism, only the portion of the cloud beneath the inversion height is considered in the NASA models, i.e., the portion of the Gaussian distributed cloud below the inversion height is used for the diffusion calculation. For model 3, it is assumed that the portion of the cloud below the inversion height is completely contained within an elliptical volume, the center of which is located at a so-called effective height. Determination of this effective height is illustrated in figure 10, in which H is the effective height, the shaded area is the effective ground cloud geometry for model 3 and Z_m is the cloud stabilization height. In model 4, the stabilized ground cloud in the mixing layer is assumed to be contained in a number of cylindrical volume sources extending from the ground to the top of the inversion height. The distribution of exhaust product concentrations in each sublayer for model 4 is assumed to be Gaussian in the alongwind and lateral directions. The total amount of product in each sublayer is given as the integration of the corresponding portion of the vertically ascending distribution cloud. Thus the predicted downwind concentrations will be very strongly dependent upon the value chosen for the inversion height.

Finally, it should be pointed out that the entrainment constant, γ, may strongly influence the predicted downwind concentrations (in addition to the selected value of the inversion height) because it influences the cloud radius which in turn affects the initial pollutant concentration distribution. Therefore the sensitivity of predicted ground level pollutant deposition to variations in entrainment constant must be studied, in addition to analyzing the available cloud rise optical data.

---

* Measurements of the mean velocity distribution in a cross section of a rising cloud from stacks show the cloud to be a double vortex. The greatest vertical velocity and buoyancy occur near the center of the cloud. As the gases encounter ambient air above the cloud, vigorous mixing occurs across the entire top of the cloud and causes the cloud diameter to grow approximately linearly with height as it rises.

2. Atmospheric Diffusion Models

The MDM is derived basically from Gaussian plume theory coupled with the Cramer diffusion coefficients. The program was originally developed for hazard estimates for the U.S. Army[27] and then adopted by Dumbauld et al[22] for NASA operation. Fundamentally, there are four models included in the program: the cylindrical distribution model 1, the static-plume model 2, the ellipsoidal distribution model 3 and the multi-layered distribution model 4. In addition, three options can be utilized within each model: precipitation scavenging, gravitational settling and surface absorption.

Briefly, model 1 assumes that the vertical distribution of pollutants is uniform and that the distributions in the alongwind and crosswind directions are Gaussian. Model 2 utilizes the same expressions as model 1 except that the dispersion process is static, i.e., the diffusion coefficients in the Gaussian distribution form are assumed constant. Model 3 is the typical three-dimensional ellipsoidal Gaussian distribution with mirror reflections on both the top and bottom boundaries. In model 4 the concentration distribution for a layer, L, is expressed as an integration of the Gaussian distributions of sublayers included in L. A damping factor is coupled with the reflection terms in models 3 and 4 to account for boundary absorption. The pollutant concentrations in different independent atmospheric physical layers can be calculated simultaneously by choosing either models 1, 2, 3, or 4 for each layer.

All models in the MDM code assume no flux of material across the physical layer boundaries. Any flux of material (which would occur if the damping factor for boundary absorption is not set equal to 1) is assumed to be instantaneously depleted. Thus the material across a layer boundary will not be accounted for in the diffusion process in the next layer when multilayer distribution is calculated simultaneously.

The Gaussian distribution assumption is only adequate for modeling the diffusion process in a quasi-homogeneous and quasi-stationary flow field with a uniform mean wind profile.[28,29] Unfortunately, the real flow field in the atmospheric boundary layer does not usually satisfy this condition. Therefore it is natural to ask whether layering the non-homogeneous or shear layer into numbers of sublayers which are nearly homogeneous and with uniform mean wind will give more accurate predictions. The answer is probably no. Although model 4 does account for the mixing of material from sublayers, its formulation is such that the material in a sublayer will spread by following its original dispersion rate in that sublayer. Thus the mixing model is not in accord with the actual physics and using model 4 with a layered atmospheric mixing layer in shear or non-homogeneous conditions will probably not give more accurate results.

3. Program Output

It should be pointed out that reference 17 gives little practical guidance on how to properly use the models for a real problem. All decisions on the operation of the code depend upon the user's familiarity with it and his knowledge of atmospheric science relating to the problem under consideration.

a. Concentration and Dosage - The total time integrated concentration at a receptor position (defined as dosage) is not directly integrated from the instantaneous concentration distribution. This is probably because it is not analytically integrable nor is it easily integrated by numerical techniques. Therefore it is important to closely examine how the dosage calculation is formulated within the code in order to clearly identify the implicit assumption associated with its use. In fact, the formulation can be obtained by either of two possible explanations. The first utilizes the classical assumption that diffusion in the alongwind direction is negligible in comparison to the gross transport by the mean wind.[30] In general, however, this assumption is not true for modeling the diffusion of self-contained rocket clouds.[31] Figure 11 demonstrates the differences in the dosage formulation between using and not using the above assumption. The lower cigar-like figure (11b) (in three dimensions it looks like a pancake) shows the model used in the MDM for the dosage calculations, which are obtained by neglecting diffusion in the X direction. The second method of interpretation which will give the identical dosage formulation is to assume that the effective instantaneous cloud during the time the cloud passes over an observer has a constant distribution which is identical to the distribution in the cloud at T_o. T_o is the time at which the cloud centroid is at the same downwind position, x, as the receptor. The latter method is also used for the formulations in MDM of the time mean alongwind concentration which is the average partial dosage from time $T_o - T_{A/2}$ to time $T_o + T_{A/2}$ over the average time T_A. Figure 12 illustrates the second assumption used for the dosage formulation. This assumption, however, is not correct because the cloud will diffuse and cannot remain uniform in turbulent flow fields. The assumption will result in a high predicted value in the near field of the launch pad. It is apparent that the time mean alongwind concentration multiplied by the time T_A is equivalent to the dosage when T_A is larger than the cloud passage time.

b. Instantaneous Concentration Distribution - The program does not produce as output an instantaneous cloud concentration distribution. Therefore any direct comparison between results calculated using the model and measured data must be made very carefully. For example, the HCl measurements for a Titan III C launch on May 20, 1975 show that concentration data at ground level were recorded at receptor locations P-9 and P-4,[20] well before the cloud centroid actually reached these locations. Therefore it is impossible to make a direct comparison between these data and the analytical results.

c. Computational Grid - The spatial resolution for calculations with the MDM code is designed for a maximum of 27,000 grid points on cylindrical coordinates, which allows the grid size to be about $\Delta X \gtrsim 1000$ m, $\Delta y \gtrsim 1500$ m, and $\Delta Z \gtrsim 2.5$ m.

4. Diffusion Coefficients

The MDM code is based in large part on the Cramer diffusion coefficients,[32-34] which are used to model the physics of atmospheric turbulent transport. Cramer assumed a power law for the diffusion coefficients which, mathematically, are the standard deviation of the pollutant particle dispersion displacement,

$$\sigma_y = \sigma_\theta \times x^p \tag{26}$$

$$\sigma_z = \sigma_\psi \times x^q \tag{27}$$

where σ_y and σ_z are diffusion coefficients in the crosswind and vertical directions, respectively and σ_θ and σ_ψ are the standard deviations of the azimuth and elevated angles, respectively.

Two sets of experimental data, from the Prairie Grass[35] and Round Hill[36] diffusion studies, were used to support Cramer's diffusion coefficients. However it should be mentioned that both the Prairie Grass and Round Hill diffusion experiments were carried out in planetary surface layers, which are usually on the order of only tens of meters. Thus, it is questionable whether the Cramer coefficients are suitable for investigating rocket ground clouds in the atmospheric mixing layer with heights on the order of hundreds to a thousand meters. At present the standard deviations σ_θ and σ_ψ of azimuth angle and elevated angle used in the MDM are calculated from an ad hoc formula[22] based on the measured σ_{θ_o} only at a reference height Z_o near the ground. These values need to be verified both theoretically and experimentally.

5. Code Operation

The total program contains about 6000 Fortran statements and 44 subroutines, most of which are for output purposes. Our experience has shown that modifications to the code will be quite difficult and could cause operational problems.

Both the cloud rise (preprocessor) program and the main MDM program were written in Fortran IV, originally for a Univac computer. Since the present operating computer system at NASA/Langley is a CDC 6600 and since there are some differences in Fortran IV software among the various computer systems, a conversion of the code to the CDC machine from the Univac system was needed. This has been accomplished on version 5 of the code and several test cases have been run successfuly using different models. The CDC version of the NASA/MSFC MDM program can be obtained from either NASA/Langley or AeroChem upon request.

B. Calculations and Comparisons with Data

A set of calculations for the cloud stabilization height, crosswind cloud width, cloud shape at stabilization and its path during cloud rise for a Titan III C launch on 20 May 1975 was made using the NASA/MSFC cloud rise models and the MDM preprocessor computer code. The results of these calculations have been compared with the available measurements carried out by the NASA/Langley Atmospheric Environments Branch.

1. Meteorological Conditions

The meteorological parametric data used in the cloud rise calculations were obtained from a rawinsonde sounding released from the Cape Canaveral weather station at launch time, 10:05 EDT. The weather was fair on the day of the launch with high pressure. The atmospheric vertical profiles of wind

velocity, temperature, wind direction and relative humidity are shown in figure 13. From these measured meteorological data collected near the launch complex at the time of launch, the inversion height appears to be at about 2203 m from the ground. In fact, the consistent sharp changes of humidity, temperature and wind velocity near 2203 m demonstrate the existence of the inversion layer. It is evident that at launch time the atmosphere was in a slightly stably stratified condition. Using Tabata's formula,[37] in which the effect of relative humidity is considered empirically, the potential temperature gradient turns out to be about 0.011 degrees K per meter.

2. Stabilization Height, Cloud Path and Comparisons with Data

Using the meteorological data mentioned above and the NASA/MSFC cloud rise models, the cloud was calculated to be stabilized at a height of 1527 m and 1664 m away from the launch pad. The total time to reach the stabilization height was about 8 min. 45 sec. The temporal history is estimated from the cloud rise formula for stable conditions in the MSFC instantaneous cloud rise models. For a Titan III C normal launch vehicle, the expression is,

$$t = \frac{1}{S^{1/2}} \left\{ \arccos \left(1 - 9.94883 \times 10^{-12} \cdot \Delta_Z\phi \cdot \rho_S \cdot Z^{3.516}\right) \right\} \qquad (28)$$

where t (sec) is the time for the exhaust cloud to rise to an altitude Z (meter). ρ_S (g/m^3) is the air density at the surface and $\Delta_Z\phi$ is the potential temperature gradient.

The stability parameter S is,

$$S = \frac{g}{T_S} \Delta_Z\phi \qquad (29)$$

where g is the gravitational constant and T_S is the surface ambient temperature. The temporal history of the ascent of the cloud mass center and the stabilization height, as well as the measured data by NASA/Langley using the Askania tracking camera, are shown in figure 14. The stabilization height and the path obtained from the NASA/Langley measurements are based on the geometric center of the cloud; the MDM code predicts the motion of the center of mass. If we assume however that the center of mass is located near the center of geometry (this occurs when the real cloud geometry is close to symmetric) direct comparisons between the calculations and data can be made because the concentration distribution in the modeled cloud is assumed to be Gaussian.

3. Cloud Width and Cloud Shape Calculations and Comparison with Data

The growing history of the cloud crosswind width during cloud rise is calculated by using the following formula, given by the NASA/MSFC cloud rise models,

$$r = \gamma Z \quad \text{for } Z \leq Z_m \qquad (30)$$

where r is the cloud radius at any height Z less than the cloud stabilization height Z_m and γ is the entrainment constant (0.64).

The cloud crosswind width history is shown in figure 15 in which the shaded area is the envelope of cloud widths from the NASA/Langley measurements for four launches.* The predicted cloud crosswind width in the initial stage apparently grows much faster than the average measured values but goes into the envelope near the cloud stabilization height.

Figure 16 shows the cloud shapes at the stabilization height. The stair-like irregular shaded area is the exhaust cloud calculated by using model 4 in the MDM preprocessor and the ellipsoidal area is from model 3. In both calculations the inversion height is set at 2203 m.

Figure 17 is scaled from real time IR measurements in a very rough manner and is given here to give a feeling for the real cloud shape. A comparison with figure 16 shows that the cloud shape calculated with model 4 gives a reasonable approximation to the measured cloud shape.

Finally, because the inversion layer cannot be exactly determined, it is important to understand the influence of using different selected values for the inversion height on the stabilized cloud shapes. When using model 4, the only change in the shape is in neglecting that portion of the cloud above the selected inversion height. When using model 3 however, the cloud shape itself will vary. As shown in figure 18 for an inversion layer at 1829 m, the cloud is compressed into a much narrower ellipse than for an inversion layer at 2203 m.

---

* The four launches are February 11, 1974, May 30, 1974, December 10, 1974 and March 14, 1976.

VI. CONCLUDING REMARKS

Based on our study of the deposition of NO_x and chlorine-containing species in the stratosphere it is concluded that:

1. Using an 'alternate' propellant in the SRM, which replaces ammonium perchlorate by ammonium nitrate in order to reduce HCl in the exhaust products, will yield approximately the same NO_x deposition rate as the baseline propellant.

2. For both baseline and 'alternate' propellants, the ratio of NO_x to chlorine-containing species deposited at 15 km and 30 km is negligibly small.

3. The Atmospheric Interaction Plume Program (AIPP) is a useful tool for computing detailed SRM plume properties.

In our study of the NASA/MSFC Multilayer Diffusion Model (MDM) for predicting SRM rocket ground cloud rise and downwind pollutant deposition it has been found that:

1. Stabilization heights calculated using the Briggs formula within the MDM code are in reasonable agreement with cloud measurements.

2. The value selected for the inversion height and the entrainment constant γ may strongly influence the downwind deposition prediction. A detailed investigation of these two parameters is needed.

3. The Cramer diffusion coefficients need to be validated for the diffusion study of the rocket generated exhaust cloud in the mixing layer.

4. The dosage and concentrations are inaccurately formulated.

5. The code requires a more definitive guideline on how to set up input data for the cloud dispersion studies.

VII. REFERENCES

1. Pergament, H.S. and Thorpe, R.D., "NO_x Deposited in the Stratosphere by the Space Shuttle," Final Summary Report, Phase I, AeroChem TN-161, NASA CR-132715, July 1975.

2. Pergament, H.S., Thorpe, R.D. and Hwang, B., "NO_x Deposited in the Stratosphere by the Space Shuttle Solid Rocket Motors," Final Summary Report, Phase II, AeroChem TP-333, NASA CR-144928, December 1975.

3. Thorpe, R.D., Pergament, H.S. and Hwang, B., "NO_x Deposition in the Stratosphere by the Space Shuttle Solid Rocket Motors," JANNAF 9th Plume Technology Meeting, CPIA Publ. 277 (Applied Physics Lab., Johns Hopkins Univ., Silver Spring, April 1976) pp. 317-352.

4. Space Shuttle Environmental Workshop on Stratospheric Effects, JSC-11137, 24-25 March 1976

5. Tokagi, T., Ogasawara, M., Fujii, K., Dazo, M., "A Study on Nitric Oxide Formation in Turbulent Flames," Fifteenth Symposium (International) on Combustion (The Combustion Institute, Pittsburgh, 1975) pp. 1051-1059.

6. Altenkirch, R.A. and Mellor, A.M., "Emission and Performance of Continuous Flow Combustors," Fifteenth Symposium (International) on Combustion (The Combustion Institute, Pittsburgh, 1975) pp. 1181-1189.

7. Mikatarian, R.R., Kau, C.J. and Pergament, H.S., "A Fast Computer Program for Nonequilibrium Rocket Plume Predictions," Final Report, AeroChem TP-282, AFRPL TR-72-94, NTIS AD 751 984, August 1972.

8. Pergament, H.S. and Kelly, J.T., "A Fully-Coupled Underexpanded Rocket Plume Program (The AIPP Code). Part I. Analytical and Numerical Techniques," Final Report, AeroChem TP-302a, AFRPL-TR-74-59, NTIS AD A006 235, November 1974.

9. Pergament, H.S. and Kelly, J.T., "A Fully-Coupled Underexpanded Afterburning Plume Program (The AIPP Code). Part II. Program User's Manual," Final Report, AeroChem TP-328, AFRPL-TR-75-52, NTIS AS A019 411, October 1975.

10. Pergament, H.S. and Thorpe, R.D., "A Computer Code for Fully-Coupled Rocket Nozzle Flows (FULLNOZ)," AeroChem TP-322, AFOSR-TR-75-1563, NTIS AD A019 538, April 1975.

11. Pergament, H.S. and Kau, C.J., "A Computer Code to Predict the Effects of Electrophilic Liquid Injection on Re-Entry Plasma Sheath Properties," Final Report, AeroChem TP-308, AFCRL-TR-74-0074, NTIS AD 782 023, January 1974.

12. Jensen, D.E., "Chamber Non-Equilibrium and Smoke Predictions for a Liquid Monopropellant Rocket Motor," JANNAF 7th Plume Technology Meeting, CPIA Publ. No. 234, June 1973.

13. Fuchs, N.A., Evaporation and Droplet Growth in Gaseous Media (Pergamon Press, London, 1959).

14. Johnstone, H.F. and Eades, D.K., Ind. Eng. Chem. 42, 2293 (1950).

15. Zebel, G., "Coagulation of Aerosols," Aerosol Science, C.N. Davies, Ed. (Academic Press, London, 1966) Ch. II.

16. Smoluchowski, M. von, Phys. Z. 17, 557, 585 (1916).

17. Dumbauld, R.K. and Bjorklund, J.R., "NASA/MSFC Multilayer Diffusion Models and Computer Programs - Version 5," NASA CR-2631, 1975.

18. Stephens, J.B., "Atmospheric Diffusion Predictions for the Exhaust Effluents from the Launch of a Titan 3C, December 13, 1973," NASA TM X-64925, 27 September 1974.

19. Lange, R., "ADPIC, A Three Dimensional Computer Code for the Study of Pollutant Dispersal and Deposition under Complex Conditions," Lawrence Livermore Lab., UCRL-5KL62, 1973.

20. Gregory, G.L., Wornom, D.C., Bendura, R.J. and Wagner, H.S., "Hydrogen Chloride Measurements from Titan III Launches at the Air Force Eastern Test Range, FL, 1973 thru 1975," NASA TM X-72832, 1976.

21. Slade, D.H., Ed., "Meteorology and Atomic Energy," USAEC-TID-24190, 1968.

22. Dumbauld, R.K. et al, ""NASA/MSFC Multilayer Diffusion Models and Computer Program for Operational Prediction of Toxic Fuel Hazards," NASA CR-129006, 1973.

23. Briggs, G.A., "Plume Rise: A Critical Survey," Air Resources Atmospheric Turbulence and Diffusion Lab., TID-25075, 1969.

24. Briggs, G.A., "Some Recent Analyses of Plume Rise Observations," presented at the Second International Clean Air Congress, Washington, DC, December 6-11, 1970, Paper ME-8E.

25. Briggs, G.A., "Discussion; Chimney Plumes in Neutral and Stable Surroundings," Atmos. Env. 6, 511-512 (1972).

26. Baker, P.J. and Jacobs, B.E.A., "Pulsed Emission Chimney," Civil Engineering Publics Work Rev., 199-200 (1971).

27. Cramer, H.E. and Dumbauld, R.K., "Experimental Designs for Dosage Prediction in CB Field Tests," Geophys. Corp. of America, GCA 68-17-G, 1968.

28. Corrsin, S., "Limitations of Gradient Transport Models in Random Walks and in Turbulence," Advances in Geophysics, Vol. 18A (Academic Press, New York, 1974) pp. 25-60.

29. Hwang, B., "Concentration Distributions in Turbulent Shear Flow," presented at 1975 Amer. Phys. Soc. Fluid Dynamics Division Annual Meeting, Univ. of Maryland, College Park, MD, 1975. (Paper submitted to J. Fluid Mech.)

30. Frenkiel, F.N., "Turbulent Diffusion: Mean Concentration Distribution in a Flow Field of Homogeneous Turbulence," Adv. Appl Mech. 3, 61-107 (1953).

31. Stephens, J.B. and Stewart, R.B., "Rocket Exhaust Effluent Modeling for Tropospheric Air Quality and Environmental Assessment," Preliminary Report, NASA, 1975.

32. Cramer, H.E., "A Practical Method for Estimating the Dispersal of Contaminants," Proceedings of the First National Conference on Applied Meteorology (Amer. Meteor. Soc., Hartford, 1957) pp. C-33 to C-35.

33. Cramer, H.E., "Engineering Estimates of Atmospheric-Dispersion Capacity," presented at Annual Meeting of the American Industrial Hygiene Association, Chicago, IL, April 1959.

34. Cramer, H.E. et al, "Meteorological Prediction Techniques and Data System," Geophysics Corp. of America, GCA-64-3-G, 1964.

35. Barad, M.L., "Project Prairie Grass. A Field Program in Diffusion," Geophysics Research Papers No. 59, Vols. I and II, AFCRC-TR-58-235, July 1958.

36. Cramer, H.E., Record, F.A. and Vaughan, H.C., Final Report, AFCRC-TR-58-239, 1958, p. 70.

37. Tabata, S., "A Simple but Accurate Formula for the Saturation Vapor Pressure Over Liquid Water," J. Appl. Meteor. 12, 1410 (1973).

TABLE I

PROPELLANT COMPOSITION

	Wt%		ΔH_f°(kcal/mole)
	Standard	Alternate	
NH_4ClO_4	69.6	10.0	-70.69
NH_3HNO_3	---	44.0	-87.27
Al	16.0	15.0	0.0
$C_{6.889}H_{10.089}O_{0.218}N_{0.264}$	12.0	---	-12.0
$C_{6.15}H_{6.97}O_{1.17}N_{0.03}$	2.0	---	-28.3
Fe_2O_3	0.4	---	-197.3
$C_4H_8N_8O_8$	---	17.0	17.9
$C_{17.6}H_{26.6}O_{0.2}$	---	12.0	13.55
$C_{22}H_{42}O_4$	---	2.0	-311.6

TABLE II

EQUILIBRIUM CHAMBER PROPERTIES

	Standard	Alternate
Pressure, Pa (N/m^2)	4.14×10^6	4.14×10^6
Temperature, K	3400	2690
Mass Fraction Al_2O_3 Particles	0.30	0.283
Gas Composition, Mole Fraction		
CO	2.49(-1)	2.71(-1)
CO_2	1.74(-2)	8.63(-3)
HCl	1.43(-1)	1.92(-2)
H	3.80(-2)	5.47(-3)
H_2	2.77(-1)	4.19(-1)
OH	9.11(-3)	2.84(-4)
H_2O	1.52(-1)	8.80(-2)
N_2	9.92(-2)	1.87(-1)
N	6.19(-6)	< 1.0(-9)
NO	7.05(-4)	1.60(-5)
O	7.45(-4)	2.45(-6)
O_2	1.62(-4)	< 1.0(-9)
Cl	1.30(-2)	1.73(-4)

TABLE III

INITIAL CONDITIONS FOR COMBUSTION CHAMBER
NONEQUILIBRIUM CALCULATIONS

Pressure	4.14×10^6 Pa (N/m^2)
Temperature	2690 K
Gas Composition, Mole Fraction	
NO	9.1(-2)
N_2	1.3(-1)
N	1.0(-10)
CO	2.6(-1)
CO_2	1.7(-4)
HCl	1.8(-2)
OH	2.7(-4)
O	2.3(-6)
O_2	2.2(-11)
Cl	1.6(-4)
H	2.2(-2)
H_2	4.7(-1)
H_2O	1.4(-4)

TABLE IV

REDUCED NO_x REACTION SET

$$K_f = AT^{-N} \exp(B/RT)$$

	A[a]	N	B (cal/mole)	Upper Bound[b]	Lower Bound[c]
$N + N + M \rightleftarrows N_2 + M$	5.5(-30)	1.0	0.0	10	10
$O + N_2 \rightleftarrows NO + N$	1.3(-10)	0.0	-76000	3	3
$N + O_2 \rightleftarrows NO + O$	2.2(-11)	0.0	6250	3	3
$NO + H \rightleftarrows N + OH$	1.5(-10)	0.0	-47000	5	5

[a] cm-molecule-sec units

[b] multiply K_f by upper bound to get upper limit of rate coefficient

[c] divide K_f by lower bound to get lower limit of rate coefficient

TABLE V

INITIAL CONDITIONS FOR AFTERBURNING CALCULATIONS

15 km, M_∞ = 1.9

	Standard	Alternate
Pressure, Pa (N/m^2)	12.21×10^3	1.22×10^4
Temperature, K	1350	1070
Velocity, m/s	2710	2410
Radius, m	8.23	8.23
Composition, Mole Fraction		
CO	2.28(-1)	2.39(-1)
CO_2	2.47(-2)	1.18(-2)
Cl	4.08(-3)	5.25(-5)
HCl	1.44(-1)	1.85(-2)
H	8.75(-3)	1.21(-3)
OH	7.21(-5)	2.20(-6)
H_2	2.74(-1)	4.03(-1)
H_2O	1.46(-1)	8.18(-2)
N_2	9.45(-2)	1.72(-1)
O	2.09(-6)	6.63(-9)
O_2	7.76(-7)	9.62(-10)
$Al_2O_3(s)$	7.46(-2)	7.21(-2)
N	9.95(-10)	9.62(-10)
NO	1.99(-4)	4.36(-6)

TABLE VI

INFLUENCE OF SHOCKS AND AFTERBURNING ON PLUME ENHANCEMENT OF NO_x

	Overall Plume Enhancement Factors (OPEF)			
	15 km		30 km	
	Baseline	Alternate	Baseline	Alternate
Shocks	3.4	216	1.5	46
Afterburning	2.5	80	1.2	10
Total	4.9	295	1.7	55

TABLE VII

NO_x DEPOSITION IN THE STRATOSPHERE (kg/s)

Nozzle	15 km	30 km
Baseline	2.5 (300 ppm)	2.5 (300 ppm)
Alternate	0.055	0.055
Plume Enhancement		
Baseline	9.5	1.5
Alternate	16.0	3.0
TOTAL		
Baseline	12.0	4.0
Alternate	16.055	3.055

TABLE VIII

COMPARISON BETWEEN NO_x AND HCl DEPOSITION RATES

15 km; Velocity = 561 m/s
30 km; Velocity = 1140 m/s

NO_x Deposition Rate (kg/m)	15 km	30 km
Baseline	0.0207	0.0036
Alternate	0.0279	0.0027
Ratio of NO_x/HCl Deposition Rates		
Baseline	0.009	0.0045
Alternate	0.099	0.0243

TABLE IX

REACTION MECHANISM FOR AIPP CALCULATIONS

$$K_f = AT^{-N} \exp(B/RT)$$

	A	N	B (cal/mole)
$O + O + M \rightarrow O_2 + M$	1.0(-29)	1.0	0.0
$O + H + M \rightarrow OH + M$	1.0(-29)	1.0	0.0
$H + H + M \rightarrow H_2 + M$	5.0(-29)	1.0	0.0
$H + OH + M \rightarrow H_2O + M$	2.0(-28)	1.0	0.0
$CO + O + M \rightarrow CO_2 + M$	1.0(-29)	1.0	-2500
$OH + OH \rightarrow H_2O + O$	1.0(-11)	0.0	-780
$OH + H_2 \rightarrow H_2O + H$	3.6(-11)	0.0	-5200
$O + H_2 \rightarrow OH + H$	2.9(-11)	0.0	-9460
$H + O_2 \rightarrow OH + O$	3.7(-10)	0.0	-16800
$CO + OH \rightarrow CO_2 + H$	9.0(-13)	0.0	-1080
$H + Cl + M \rightarrow HCl + M$	5.5(-31)	1.0	0.0
$HCl + OH \rightarrow H_2O + Cl$	7.2(-12)	0.0	-3250
$H + HCl \rightarrow Cl + H_2$	8.8(-11)	0.0	-4620
$OH + Cl \rightarrow HCl + O$	3.0(-11)	0.0	-5000
$O + N_2 \rightarrow NO + N$	1.3(-10)	0.0	-76000
$N + O_2 \rightarrow O + NO$	2.2(-11)	0.0	-6250
$NO + H \rightarrow N + OH$	1.5(-10)	0.0	-47000
$N + N + M \rightarrow N_2 + M$	5.5(-30)	1.0	0.0

TABLE X

HETEROGENEOUS REACTION MECHANISM

(one way reactions only)

$$H + OH + S \rightarrow H_2O + S$$
$$O + H + S \rightarrow OH + S$$
$$O + O + S \rightarrow O_2 + S$$
$$H + H + S \rightarrow H_2 + S$$
$$CO + O + S \rightarrow CO_2 + S$$
$$H + Cl + S \rightarrow HCl + S$$
$$Cl + Cl + S \rightarrow Cl_2 + S$$
$$N + N + S \rightarrow N_2 + S$$
$$N + O + S \rightarrow NO + S$$

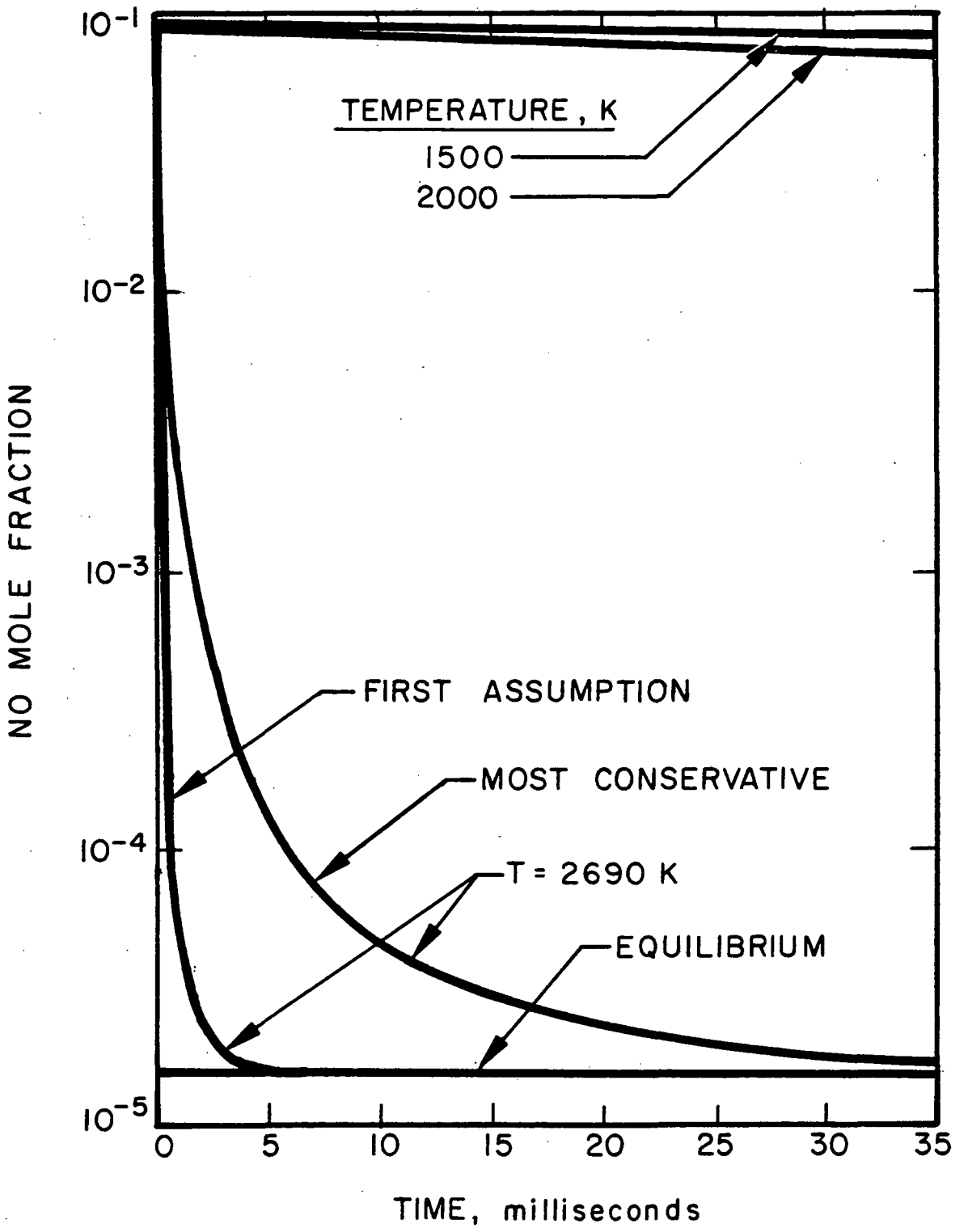

Figure 1. Approach to equilibrium of NO_x in SRM combustion chamber.

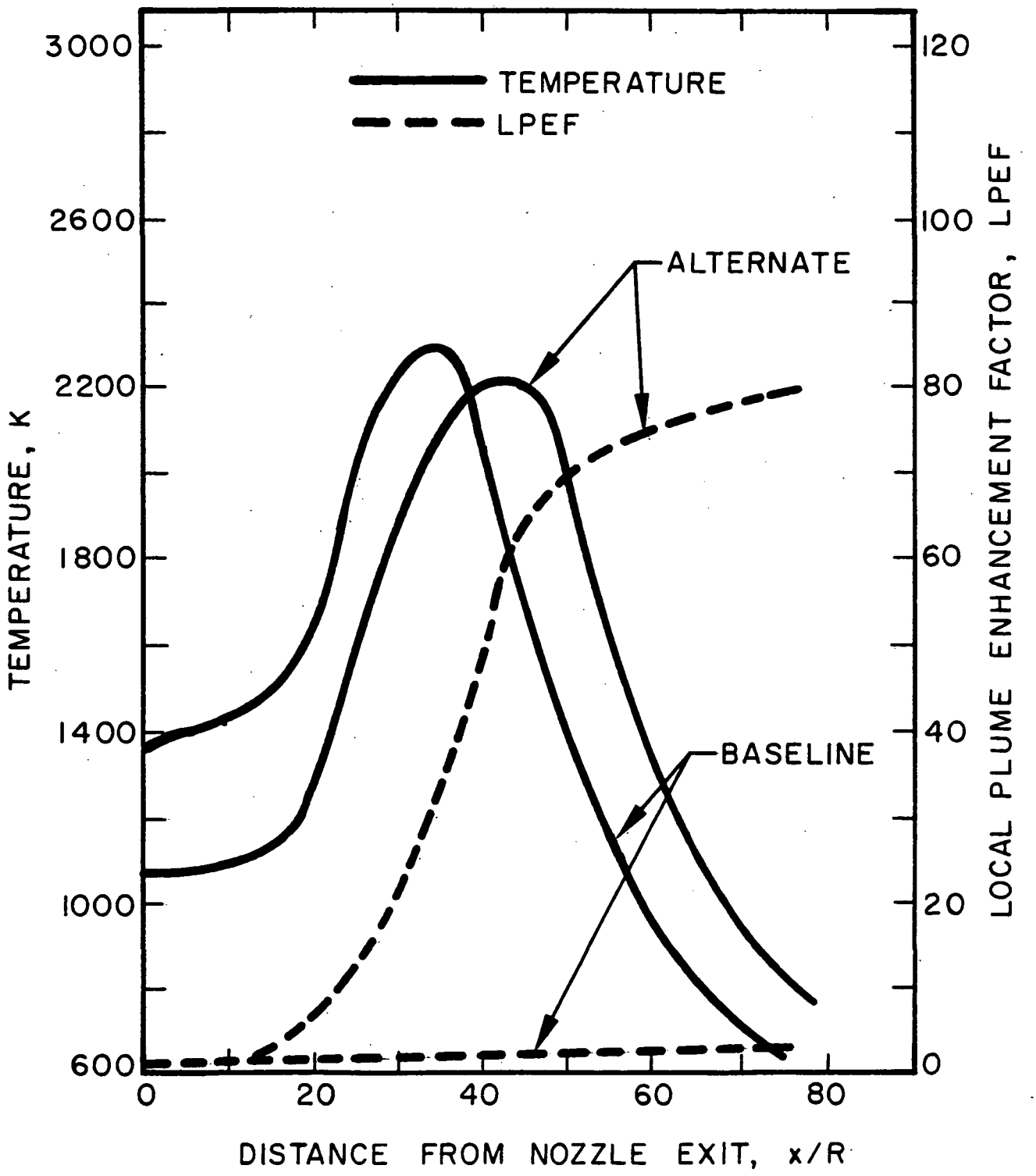

Figure 2. Influence of afterburning on plume temperatures and NO_x enhancement.
Baseline and Alternate propellants, 15 km

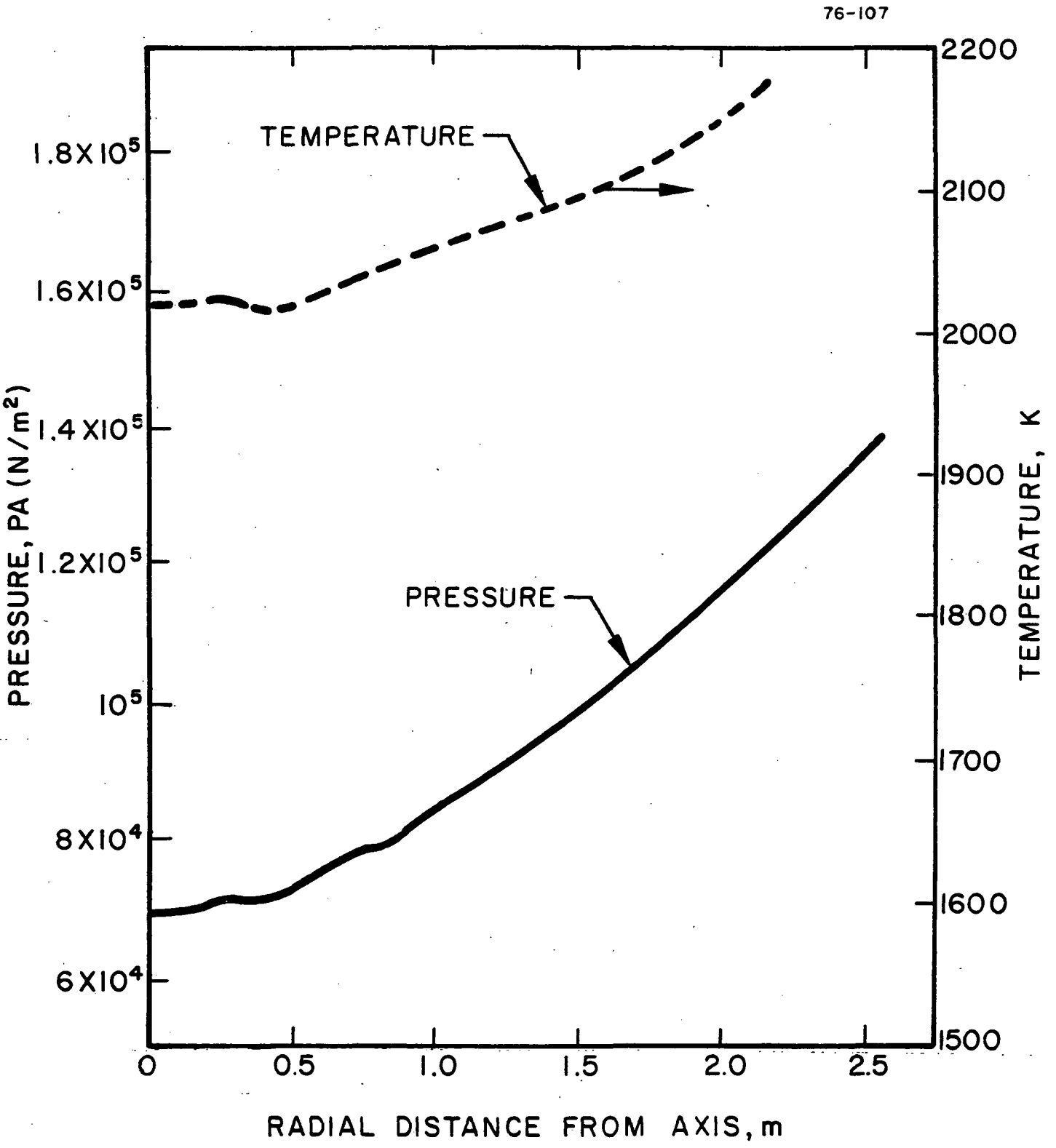

Figure 3. SRM nozzle exit plane pressure and gas temperature distributions.

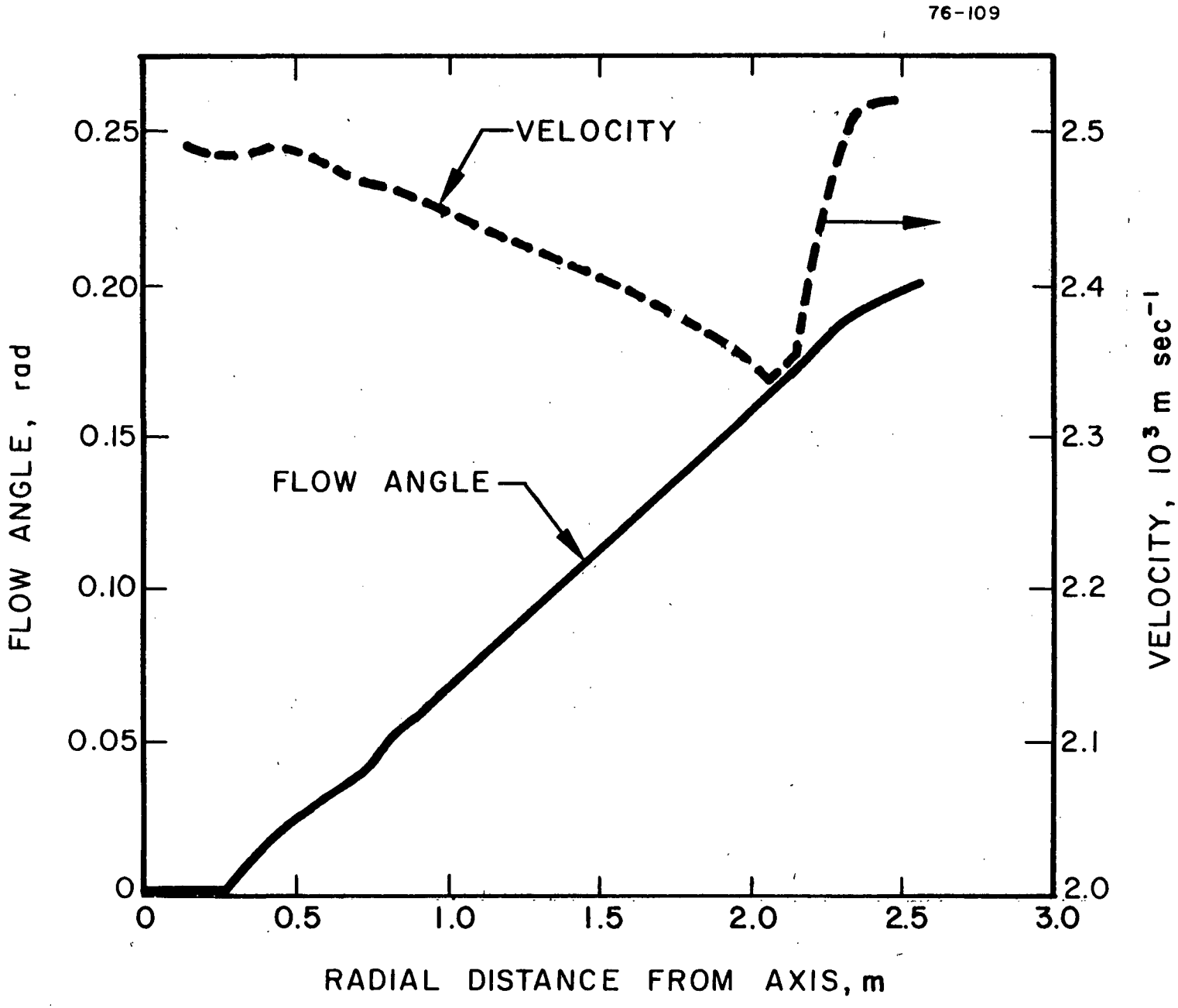

Figure 4. SRM nozzle exit plane gas velocity and flow angle distributions.

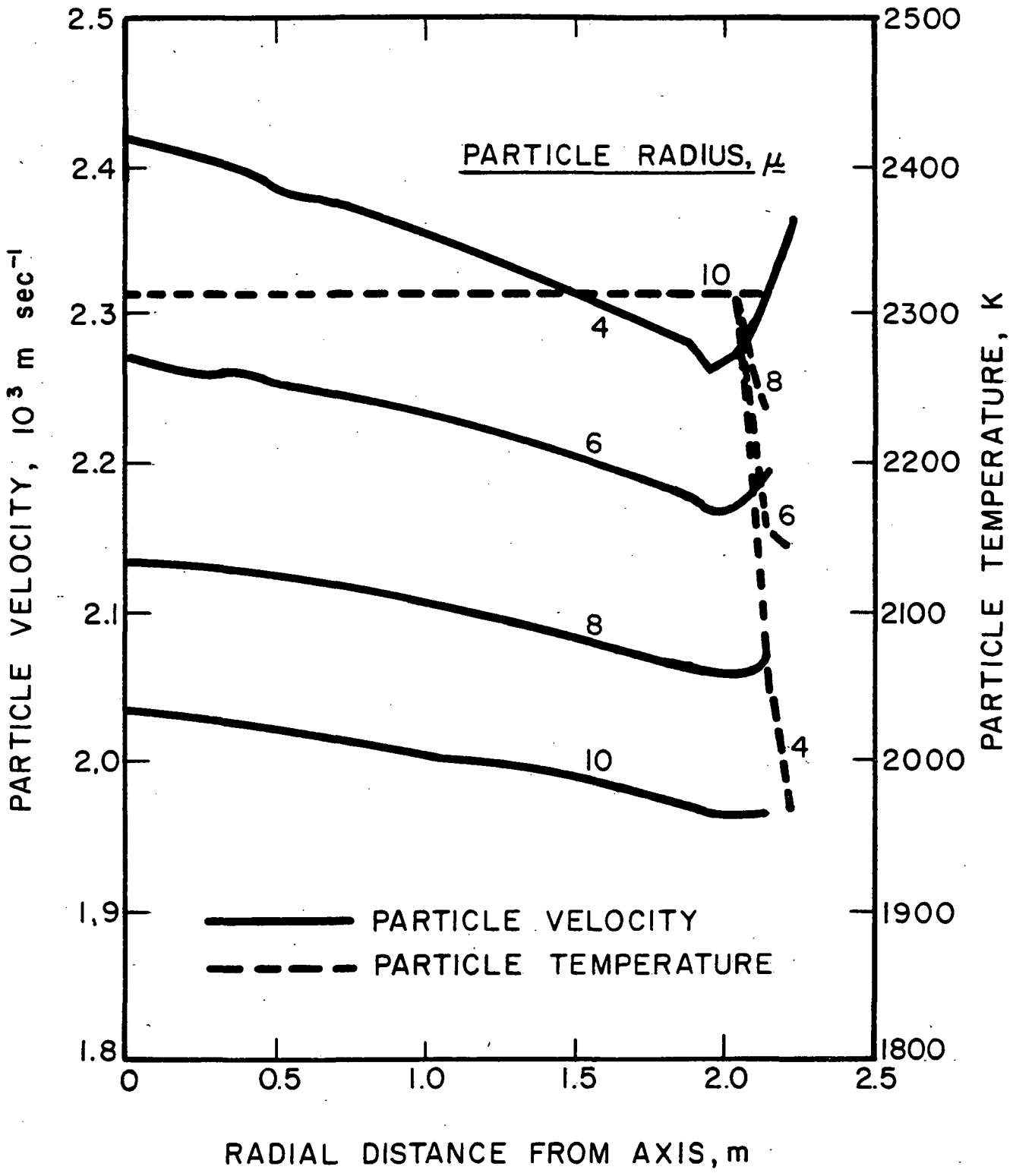

Figure 5. SRM nozzle exit plane particle temperature and velocity distributions.

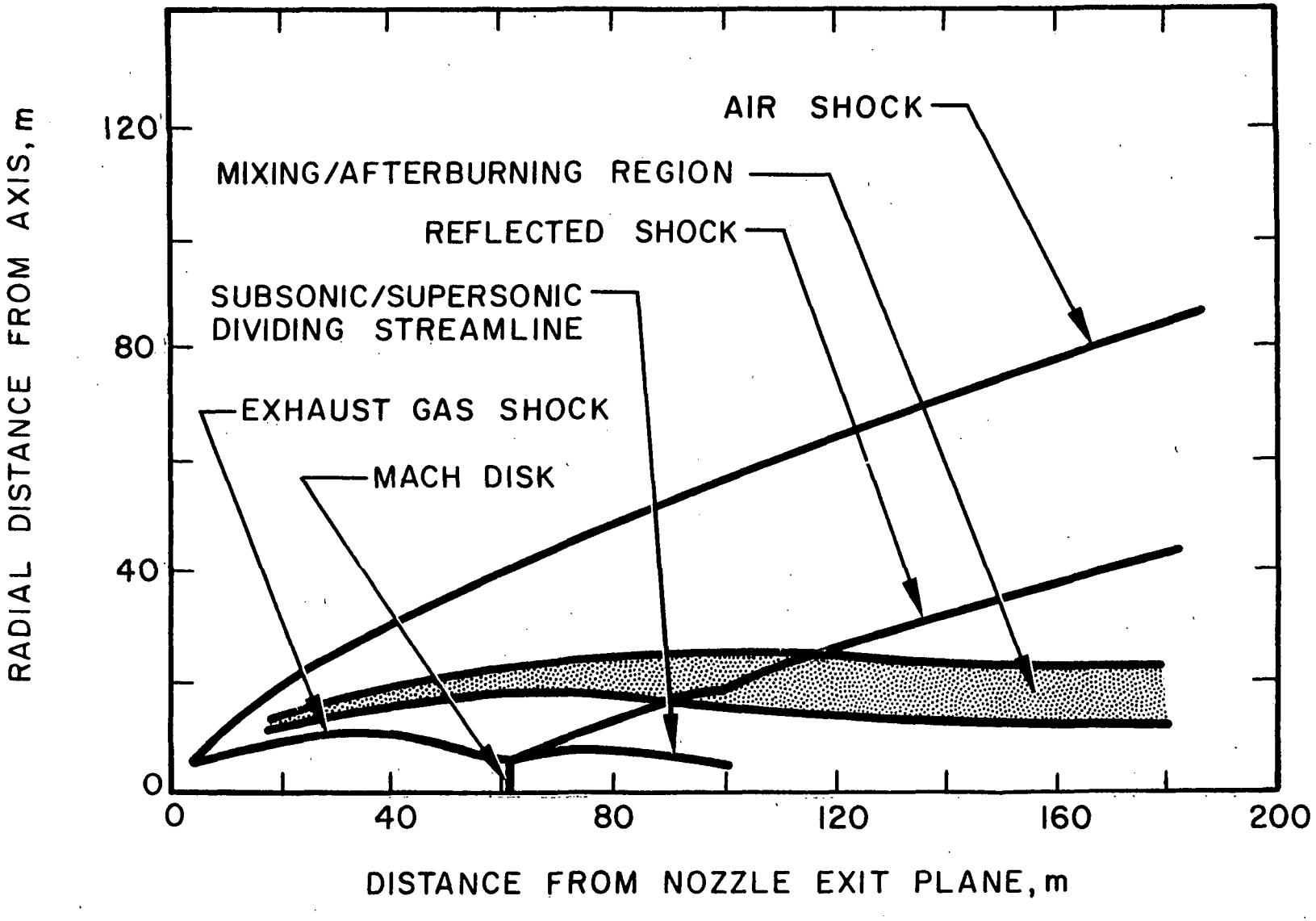

Figure 6. SRM exhaust plume structure. 30 km, vehicle Mach number = 3.8. Mixing region outer boundary defined as ambient N_2 less 5% of the difference between ambient and exhaust product N_2; inner boundary is exhaust product N_2 plus 5% of the difference.

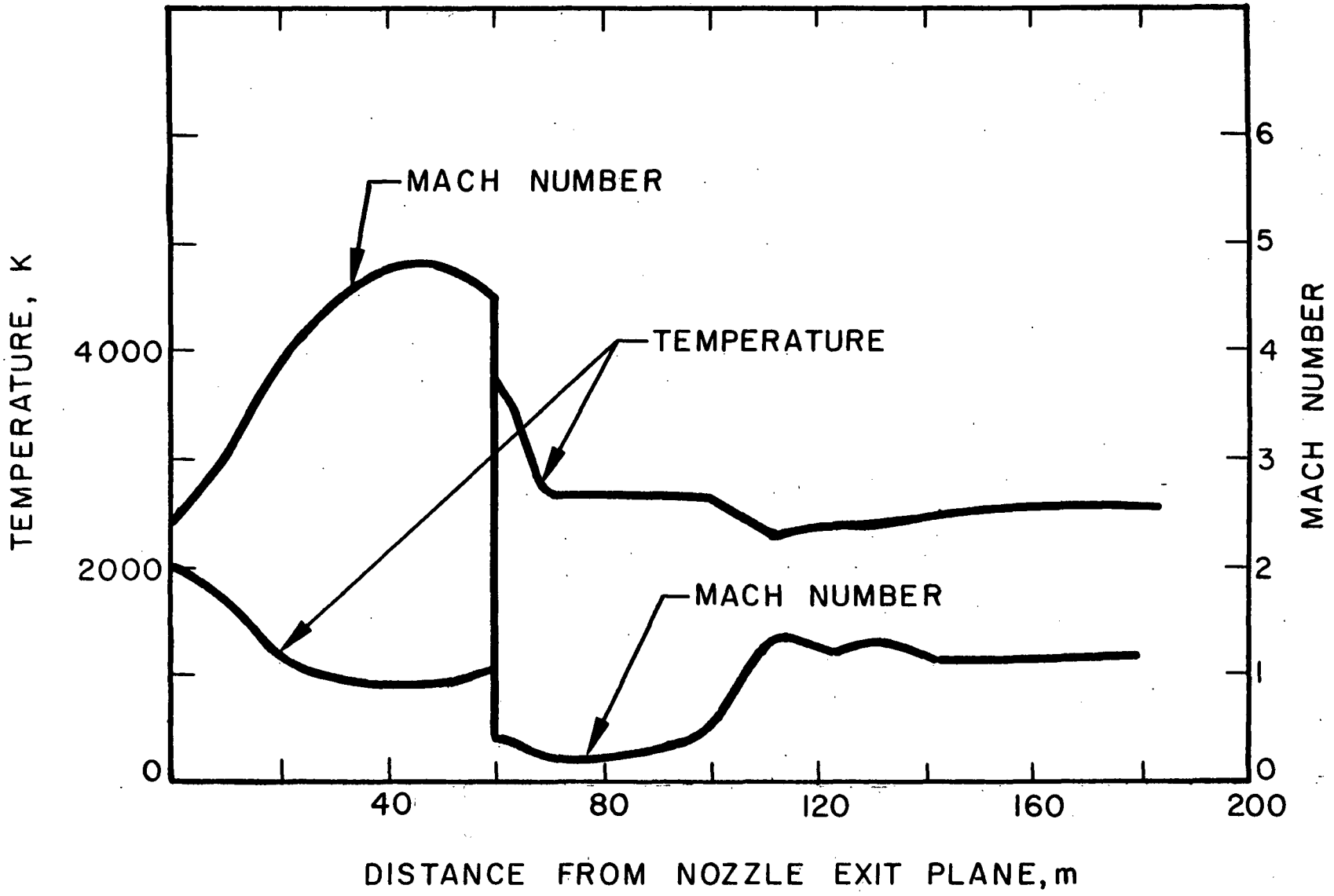

Figure 7. SRM exhaust plume centerline temperature and Mach number distributions.

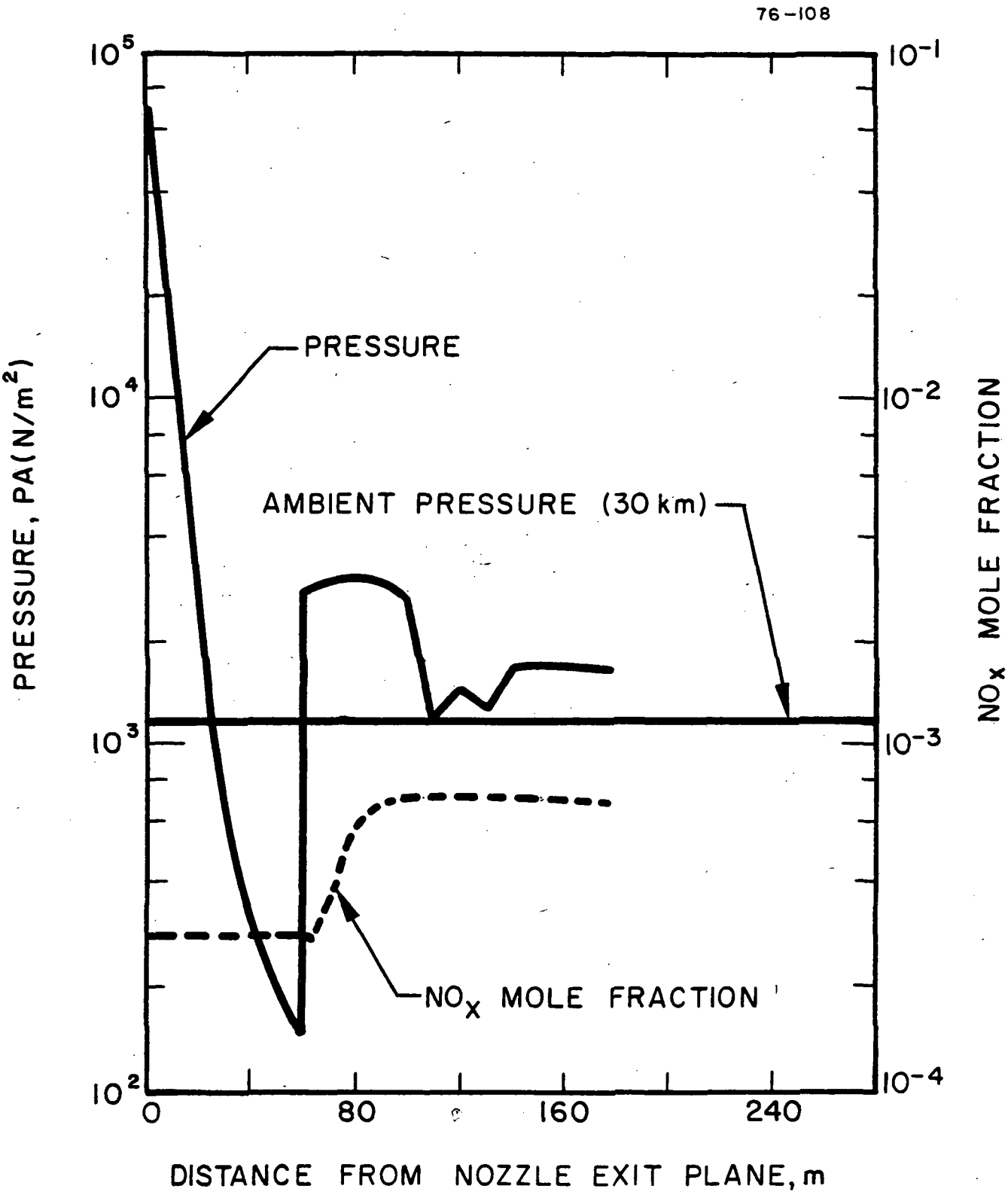

Figure 8 SRM exhaust plume centerline pressure and NO_x mole fraction distributions.

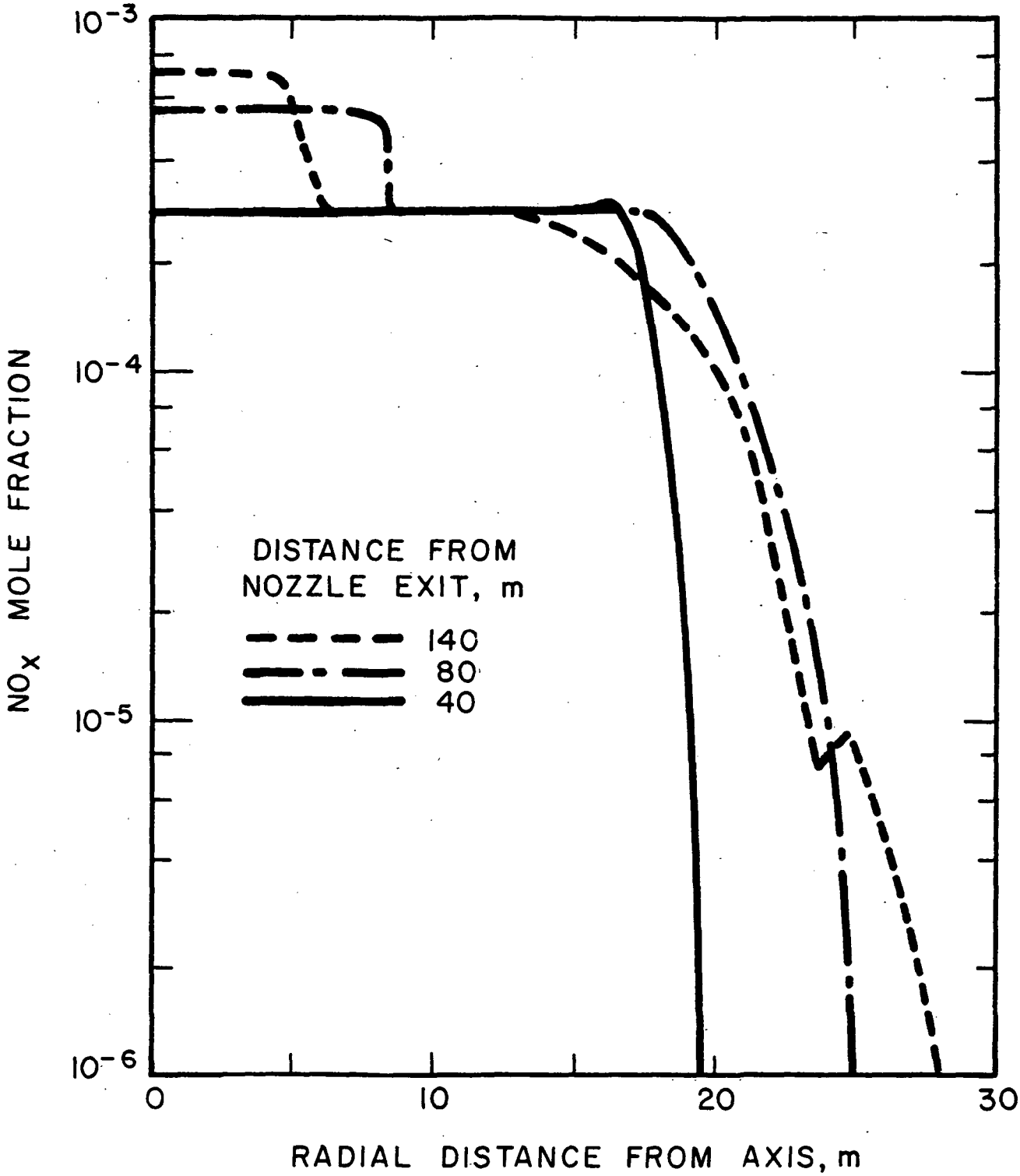

Figure 9. Radial NO_x profiles in SRM plume at 30 km.

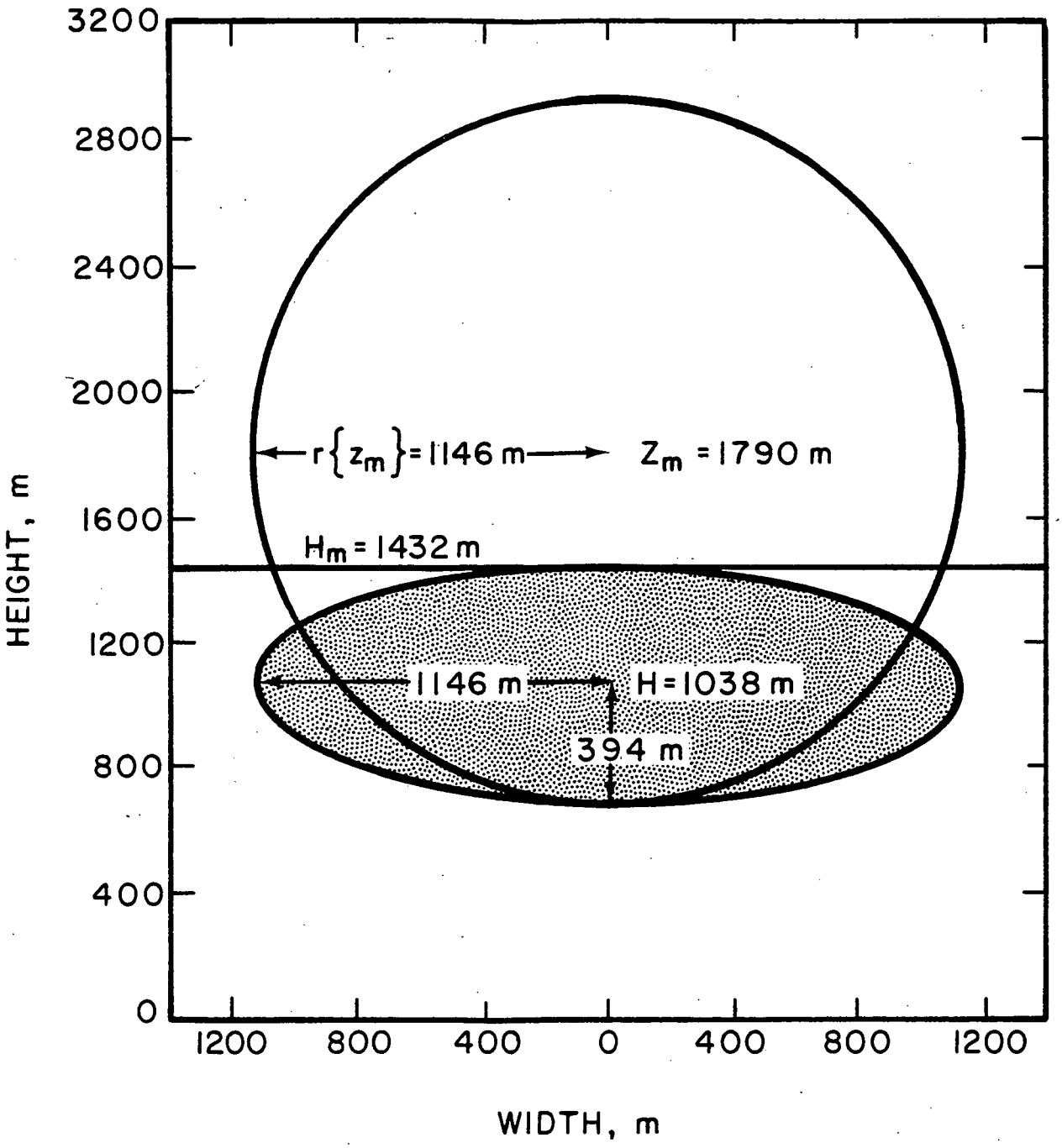

Figure 10. Configuration of stabilized cloud of exhaust products used for model 3 calculation (for a simulated normal launch of Space Shuttle vehicle on 21 October 1972). Shaded area represents effective cloud dimensions, H_m is inversion height.

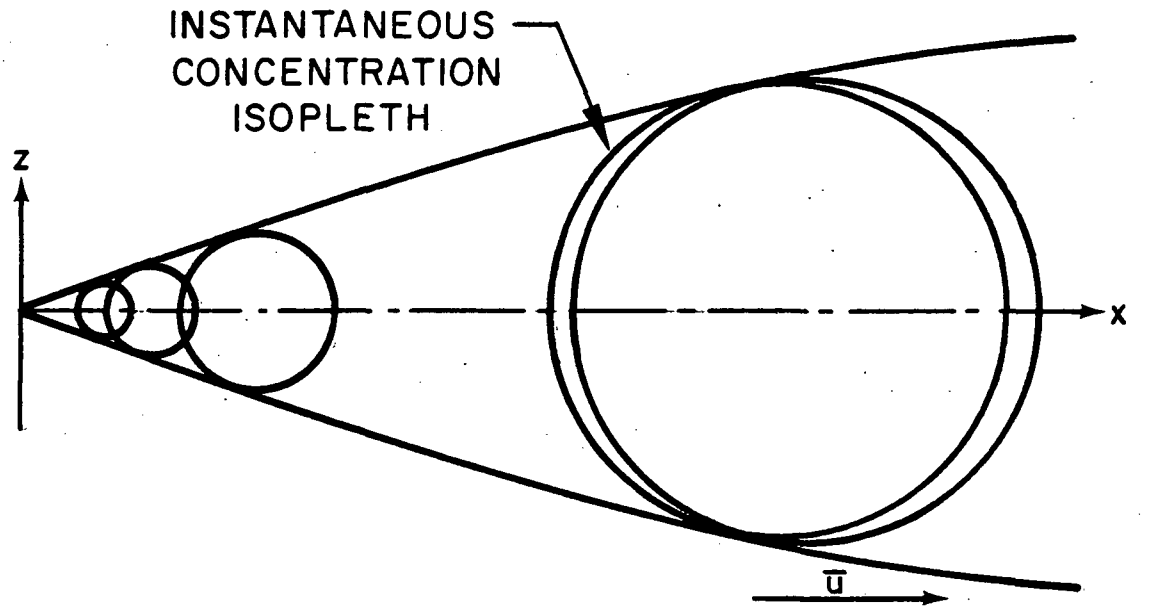

Figure 11a. Schematic formation of plume from superposition of individual instantaneous concentrations at subsequent times.

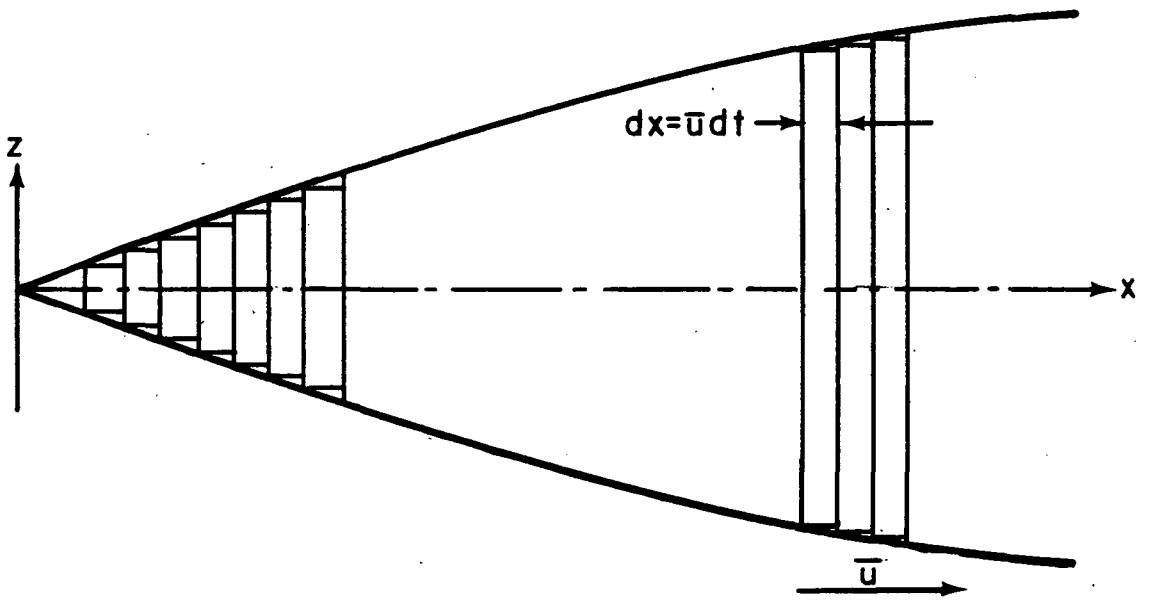

Figure 11b. Schematic spreading-disc plume model neglecting X-diffusion.

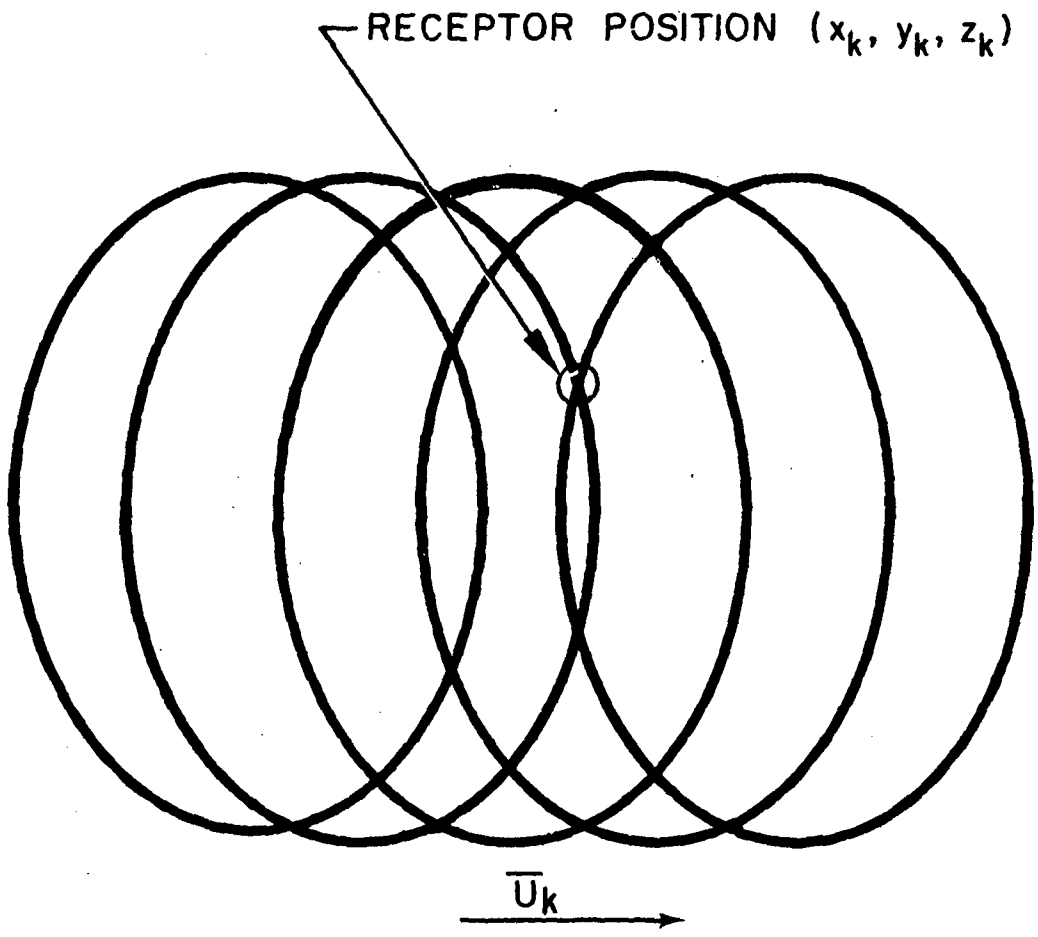

Figure 12. Schematic formation of time integrated concentration. Constant concentration distributions assumed during the time cloud passes the receptor.

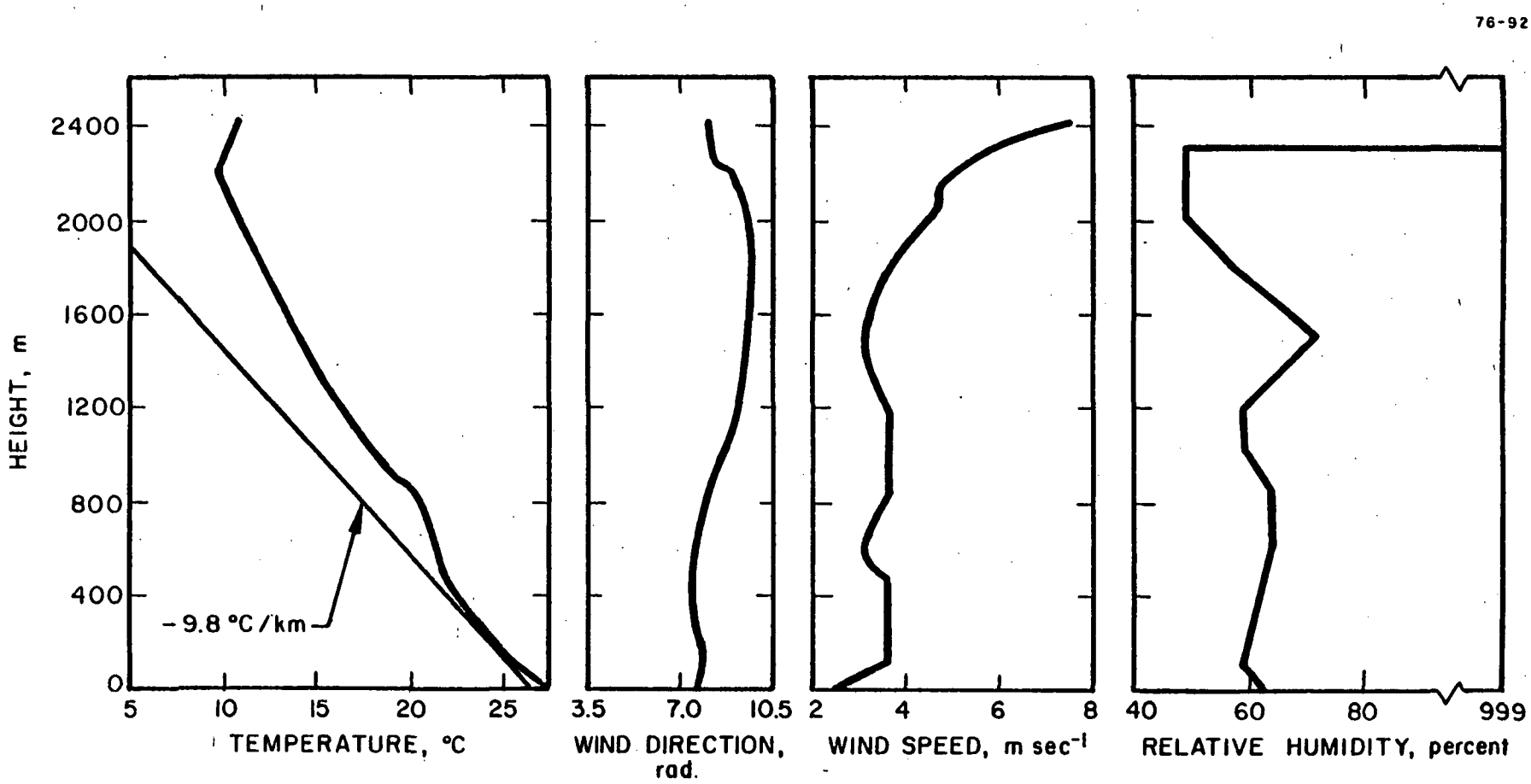

Figure 13. Vertical profiles of temperature, wind speed, wind direction and relative humidity at Kennedy Space Center from rawinsonde sounding measurement for 20 May 1975, 10:05 EDT.

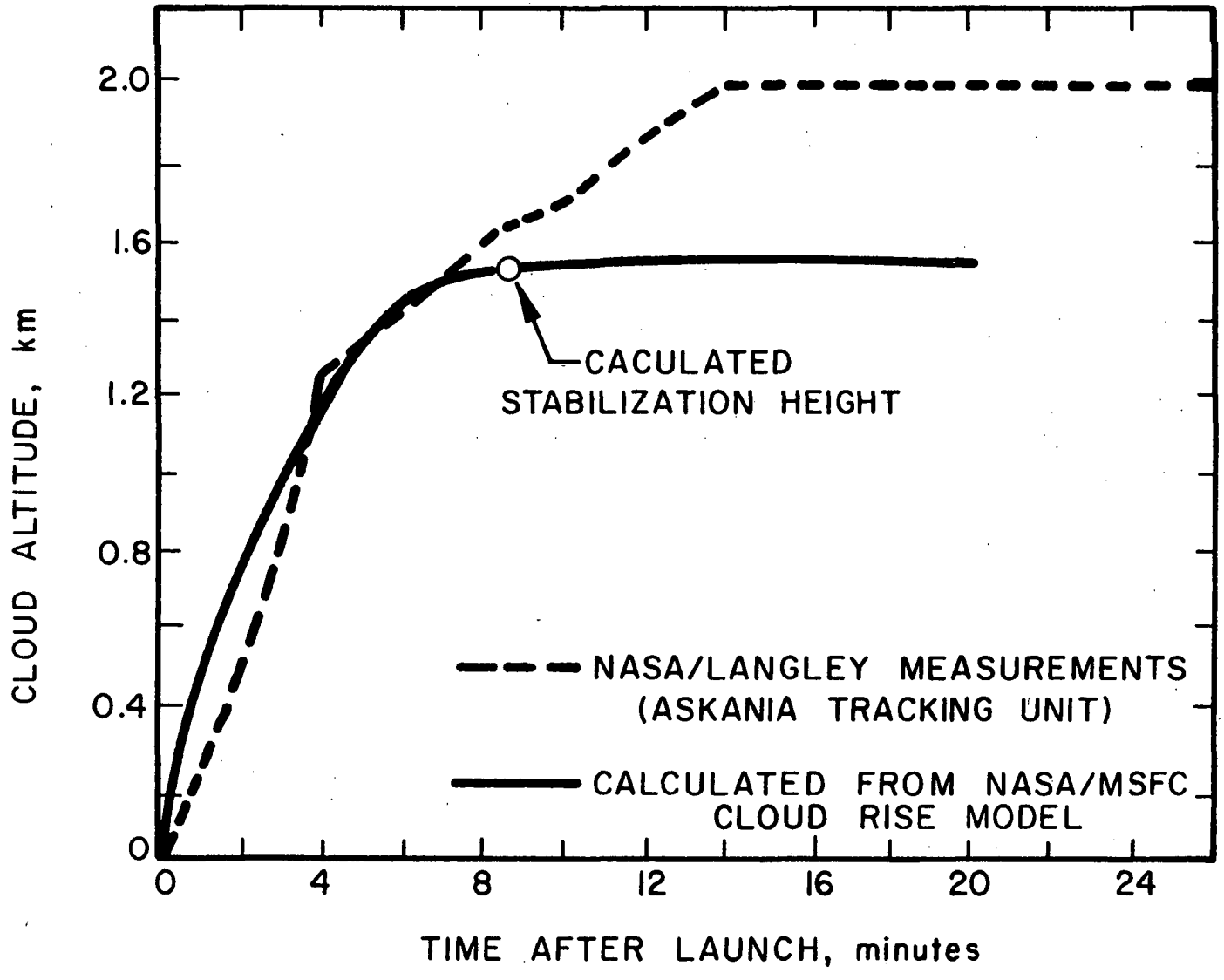

Figure 14. Comparison of the path of rising cloud obtained from optical measurements and the NASA/MSFC cloud rise model for a Titan III C vehicle on 20 May 1975.

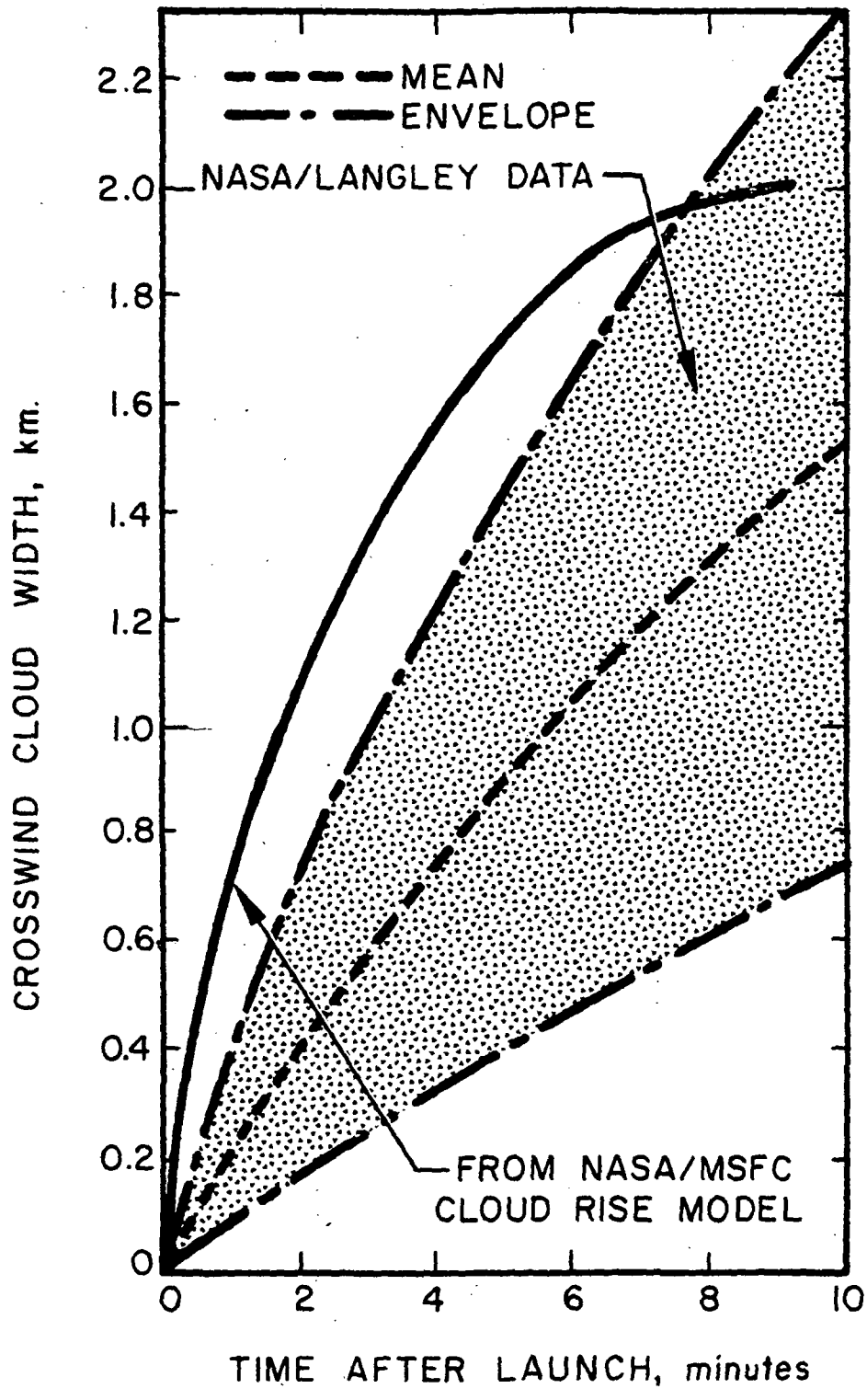

Figure 15. A comparison between calculated and measured crosswind cloud widths.

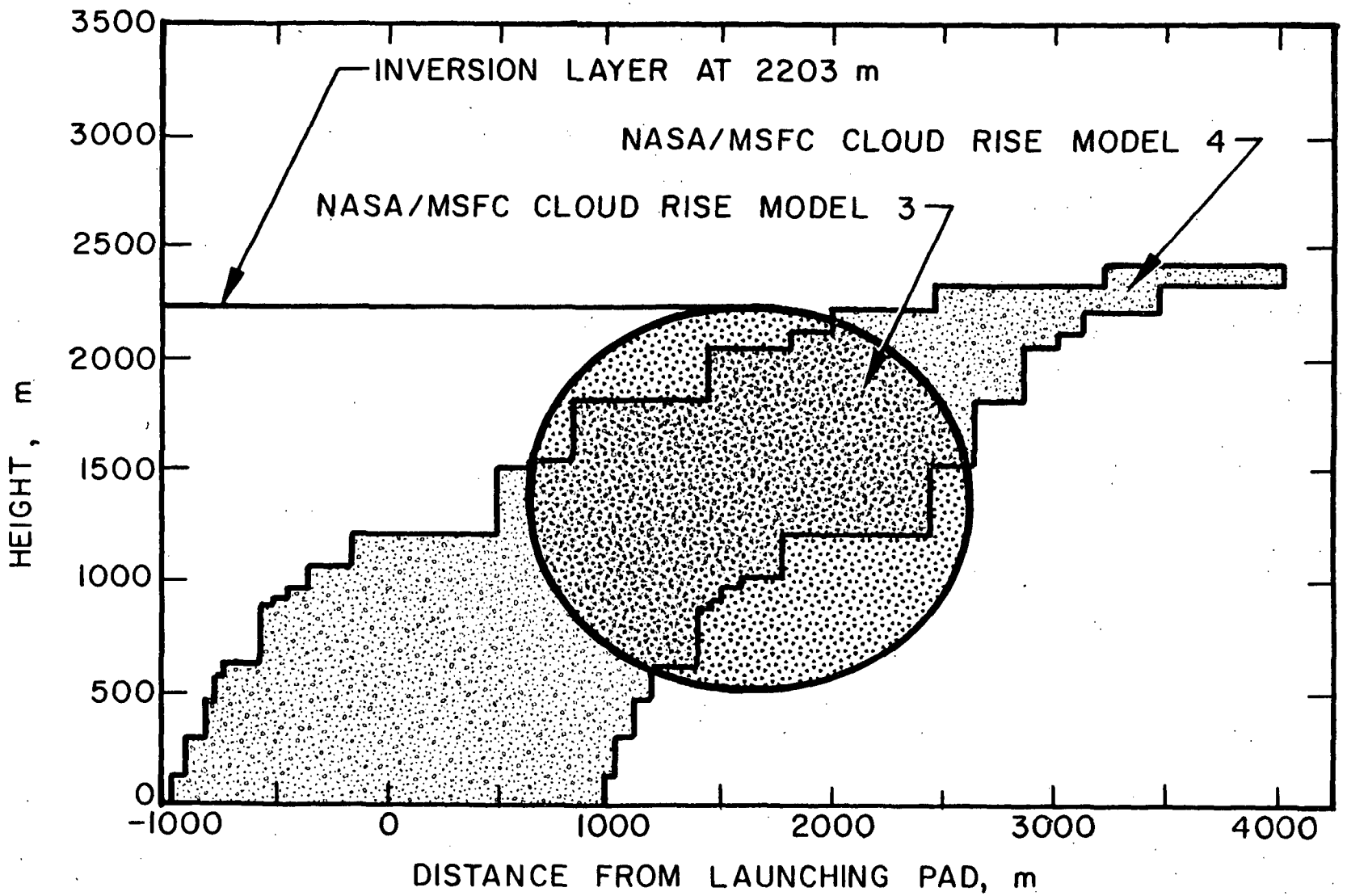

Figure 16. Stabilized cloud configuration obtained from NASA/MSFC cloud rise models 3 and 4.

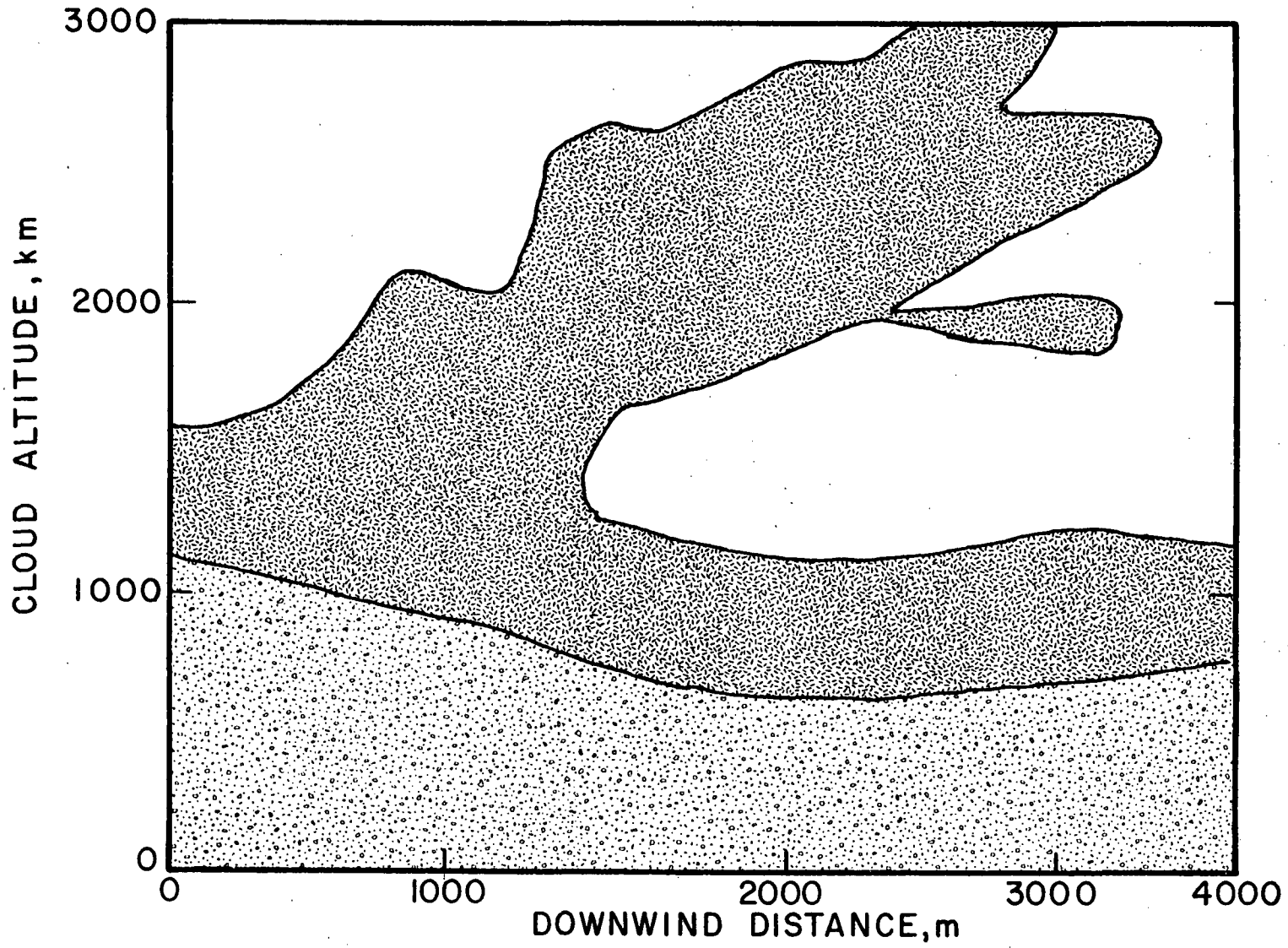

Figure 17. Cloud configuration 17 min. after Titan III C launch, 20 May 1975. (from NASA/Langley IR measurements)

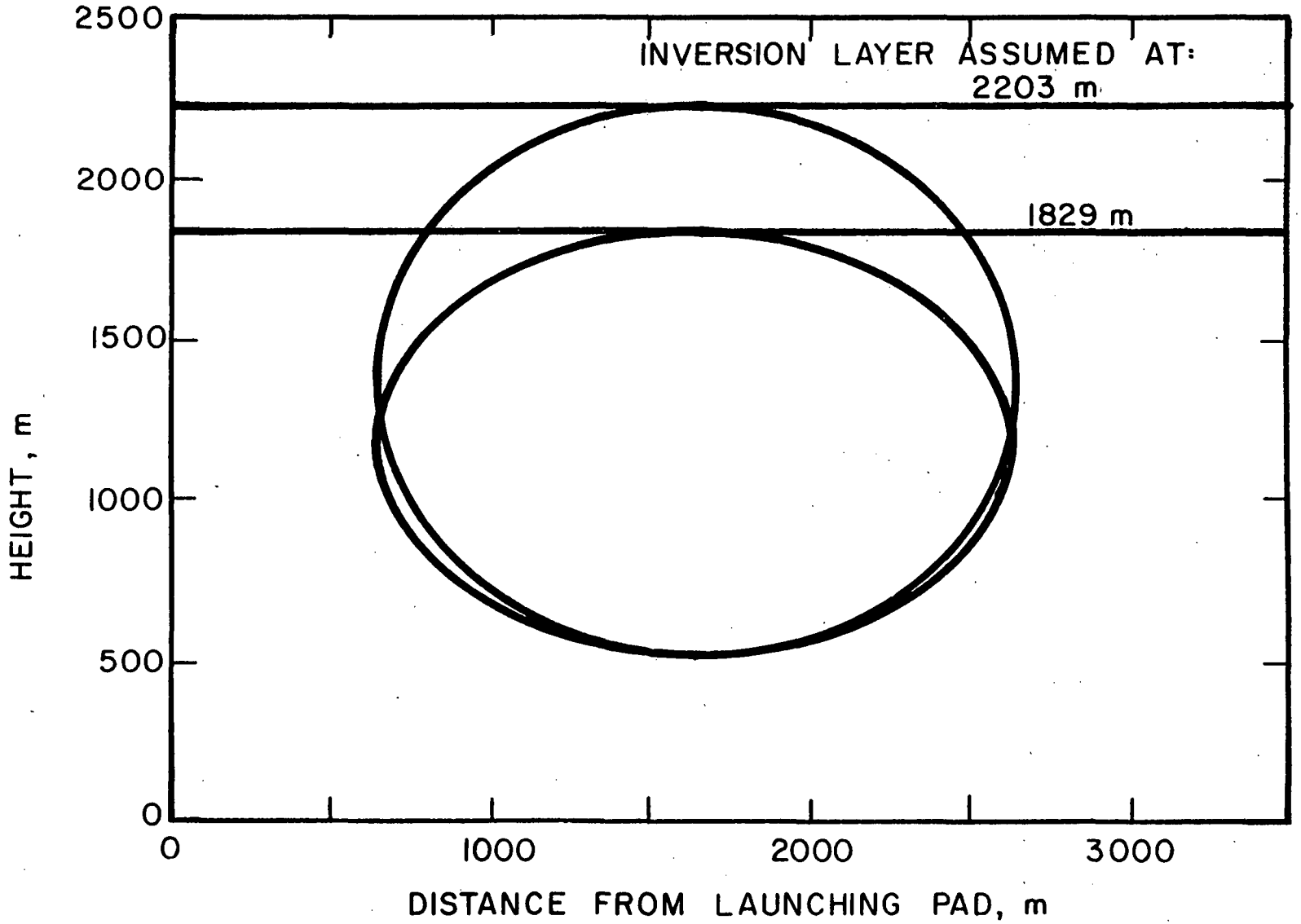

Figure 18. Effective cloud configurations calculated from NASA/MSFC cloud rise model 3 using different inversion heights.